International
Progress Report

IPR-01-27

Äspö Hard Rock Laboratory

TRUE Block Scale project

Investigation of porosity and micro-fracturing in granitic fracture wall rock and fault breccia specimens using the PMMA technique

Maarit Kelokaski
Esa Oila
Marja Siitari-Kauppi

University of Helsinki

August 2001

Svensk Kärnbränslehantering AB
Swedish Nuclear Fuel
and Waste Management Co
Box 5864
SE-102 40 Stockholm Sweden
Tel +46 8 459 84 00
Fax +46 8 661 57 19

Äspö Hard Rock
Laboratory

Report no.
IPR-01-27

No.
F56K

Author
Kelokaski, Oila, Siitari-Kauppi

Date

Checked by
Anders Winberg

Date
01-08-30

Approved
Christer Svemar

Date
01-09-18

Äspö Hard Rock Laboratory

TRUE Block Scale project

Investigation of porosity and microfracturing in granitic fracture wall rock and fault breccia specimens using the PMMA technique

Maarit Kelokaski
Esa Oila
Marja Siitari-Kauppi

University of Helsinki

August 2001

Keywords: Autoradiography, fault breccia, fracture, micro fractures, PMMA, porosity, porosity distributions, porosity profile, TRUE Block Scale, wall rock, microfracturing

ABSTRACT

The objective of the work was to analyse the porosity and microfracturing of ten samples from interpreted deterministic structures at the TRUE Block Scale Site using ^{14}C-PMMA method. The work comprised analysis of three categories of rock samples: Fault breccia material (fragments and pieces) and wall rock samples.

The ^{14}C-PMMA method involves impregnation of rock samples with ^{14}C-labelled methylmethacrylate (^{14}C-MMA) in a vacuum, irradiation polymerisation, sample preparation and partitioning, autoradiography, optical densitometry and porosity calculation routines using digital image processing techniques. In the work ^{3}H labelled methylmethacrylate was used for some of the fragment samples. The advance of the ^{3}H is its low beta energy (18 keV) allowing autoradiography of very thin rock samples.

Methylmethacrylate intruded into dark minerals of the fault breccia fragment samples taken from two intercepts; structure # 22 in KI0025F02:66.7m and structure #20 in KI0023B:69.9m. Porosities of several percents were determined. MMA had distributed homogeneously inside dark mineral grains according to the visual inspection of the autoradiographs. When MMA had intruded into the feldspar mineral grains, porosity distribution was heterogeneous, even cracks and fissures could be distinguished on the autoradiograph from the 1-2 mm size fragments. Some of the feldspar grains were nonporous with the PMMA method.

A total amount of four samples of fault breccia pieces were impregnated with ^{14}C-MMA. The samples were taken from two intercepts: structure # 22 in KI0025F02:66.7m and structure #20 in KI0023B:69.9m. Total porosity of piece structure # 22 in KI0025F02:66.7m was around 0.6 % and that of piece structure #20 in KI0023B:69.9m was around 0.7 %. Fault breccia pieces contained plenty of cracks and fissures having apertures between 10 to 20 µm.

Six wall rock samples were impregnated with ^{14}C-MMA. The porosity pattern of samples taken from intercepts structure # 22 in KI0025F02:66.7m and structure #20 in

KI0023B:69.9m included cracks and fissures. Dark and altered minerals had the highest porosities; around 6 to 8 %. Very tight altered mineral phases proved to be nonporous with the PMMA method. Wall rock samples of intercepts structure # 23 in KI0025F03:56.8m and structure #21 in KI0023F:71.1m had total porosities of around 0.3 % with the PMMA method. Porous mineral grains and open mineral grain boundaries form connected migration pathways. The feldspar grains are slightly porous; a few microcracks and fissures transsect large potassium feldspar phenocrysts. The porosity pattern of sample taken from intercept structure #20 in KI0025F02:74.6m contained porous veins (porosity around 1 %) cutting the core sample parallel to the fracture surface. The MMA didnot intruded completely into the wall rock sample taken from an intercept structure #20 in KA2563:188.7m. Contrary to the conditions seen in the other wall rock samples, feldspars here showed porosity of 0.35 %. A strongly altered mylonitic phase adjacent to the fracture surface was not impregnated with MMA.

PREFACE

The work was carried out by Maarit Kelokaski, Esa Oila and Marja Siitari-Kauppi at the Laboratory of Radiochemistry, Department of Chemistry, of the University of Helsinki. The work described here is carried out to study the porosity and microfracturing in ten samples taken from interpreted deterministic structures in a dioritic host rock taken from the TRUE Block Scale Site at the Äspö Hard Rock Laboratory.

The work was commissioned by Aimo Hautojärvi of Posiva Oy and Anders Winberg of Conterra AB on behalf of SKB under contract no. 9713/00/AJH.

1. INTRODUCTION

The objective of the activity was to determine the porosity and microfracturing of altered Äspö diorite samples from the interpreted deterministic structures at TRUE Block Scale Site by using the ^{14}C-PMMA method (^{14}C-polymethylmethacrylate method). The visualisation and quantitative results on interconnected porosity of rock samples, mineral specific porosities of main minerals, porosity profiles of altered zones next to water conducting fractures and microfracturing was studied. Three categories of rock samples e.g. fault breccia fragments (1-2 mm), fault breccia pieces (1-3 cm) in the following denoted "fragments" and "pieces" and wall rock samples, were studied by using ^{14}C-PMMA method.

The ^{14}C-PMMA method involves impregnation of rock samples with ^{14}C-labelled methylmethacrylate (^{14}C-MMA) in a vacuum, irradiation polymerisation, sample partitioning, autoradiography, optical densitometry and porosity calculation routines using digital image processing techniques. In the work ^{3}H labelled methylmethacrylate was used for some of the fragment samples. The advantage of the ^{3}H compared to ^{14}C is its low beta energy (18 keV) allowing autoradiography of very thin rock samples. The rock samples used in the PMMA analyses are listed in Table I.

Table I. List of rock samples analysed in study.

code	classification	priority
#22 KI0025F02:66.7m	wall rock	**1**
#22 KI0025F02:66.7m	2 wall rock pieces	**1**
#22 KI0025F02:66.7m	fragments	**1**
#22 KI0025F02:66.7m	fragments/test	**1**
#23 KI0025F03:56.8m	wall rock	**2**
#20 KI0023B:69.9m	wall rock	**3**
#20 KI0023B:69.9m	2 wall rock pieces	**3**
#20 KI0023B:69.9 m	fragments	**3**
#20 KI0023B:69.9m	fragments/test	**3**
#21 KI0023F:71.1m	wall rock	**4**
#20 KI0025F02:74.6m	wall rock	**5**
#20 KA2563:188.7m	wall rock	**6**

2. EXPERIMENTAL

2.1 Fault breccia fragments

"Fragments" were 0.5-1 and 1-2 mm sized rock particles constituting a fraction of a fault breccia from two intercepts structure #22 in KI0025F02:66.7m and structure #20 in KI0023B:69.9m. Fragments having grain size of 0.5-1 mm were planned to be used for testing the method. This first category of samples required tests for optimizing the impregnation + autoradiography procedure.

The fragments were dried in a vacuum chamber in glass vials using a maximum temperature of 120 °C. The fragments were impregnated first with ^{14}C labelled methylmethacrylate. ^{3}H labelled methylmethacrylate was tried for some of the fragment samples. Polymerization of methylmethacrylate was initiated with a Co-60 gamma radiation source. The samples were surrounded by radioactive methylmethacrylate to avoid outdiffusion of tracer into lower concentration during radiation.

The penetration range of beta particles of ^{3}H (around 3 µm) is lower in the rock matrix due to lower beta energy (18 keV) than the range of beta particles of ^{14}C (around 100 µm) having beta energy of 155 keV. When the fragments are embedded into radioactive PMMA the penetration range of beta particles of ^{14}C would cause blackening of autoradiograph through the thin rock layer. To avoid this artefact the tracer ^{3}H-MMA was employed. The autoradiographs of fragments were analysed partly through microscope+CCD camera to utilize the impoved resolution of of autoradiographs. Fragments were embedded with MMA and polymerized MMA act as mantle for the fragments during preparation of the samples for autoradiography by grinding or sawing.

The fragments tested in the present study are listed in Table II, where the grain sizes, used weights of particles in each test, the sample priority, the experiment codes and the ^{3}H- and ^{14}C-MMA tracer activities are listed. The detailed experimental steps are listed in Appendix 1, where drying, impregnation and autoradiography are shown for each test. The test3 sample was sawn into two parts with the Isomet Low Speed Saw after polymerization, but

other test samples were only grinded with grinding paper and polished with the silicon carbide grinding powder (400 mesh).

Table II. Fault breccia fragments - grain sizes, weights of particles, sample priority, experiment codes and ^{3}H- and ^{14}C-MMA tracer activities.

	grain size (Æ mm)	weight (g)	priority	experiment code	tracer activity
^{14}C-PMMA					
#22 KI0025F02:66.7m	0.5-1.0	0.0758	1	test1	0.7µCi/ml
#22 KI0025F02:66.7m	0.5-1.0	0.1254	1	test2	0.7µCi/ml
#22 KI0025F02:66.7m	1-2	0.6533	1	test 3	1.2µCi/ml
#22 KI0025F02:66.7m	1-2	0.2077	1	test 4	25µCi/ml
3H-PMMA					
#22 KI0025F02:66.7m	1-2	0.2319	1	test 5	3 mCi/ml
#20 KI0023B:69.9m	0.5-1.0	0.0731	3	test 6	3 mCi/ml
#20 KI0023B:69.9m	1-2	0.1607	3	test 7	3 mCi/ml

2.2 Fault breccia pieces

"Pieces" were sugar-cube sized (∅ 1-2 cm) fraction of a fault breccia, which had been collected using a triple tube core barrel. The total amount of pieces samples was 4. Two of them represented the intercept structure #22 in KI0025F02:66.7m (A and B) and two of them the intercept structure #20 in KI0023B:69.9m (A and B).

The pieces were dried in a vacuum chamber using maximum temperature of 70 °C for pieces B and that of 120 °C for pieces A. In the author's experience the rock samples for PMMA measurements are dried first using as mild drying conditions as possible to avoid any increased porosity in the rock samples. Here the first impregnation using low drying temperature and low tracer activity did not succeed and the drying temperature as well as the tracer activity were increased in the case of pieces A samples. The pieces were impregnated with ^{14}C labelled methylmethacrylate. The pieces samples from both intercepts were irradiated with radioactive methylmethacrylate as outer solution to avoid

outdiffusion of tracer into lower concentration during radiation. This category of samples were sawn into two with the Isomet Low Speed Saw.

The pieces studied here are listed in Table III, where the weights of pieces, the sample priority and the ^{14}C-MMA tracer activities are listed. The porosity values of two parallel "pieces" samples were determined with the water saturation technique and these values are also listed in Table III. The detailed experimental steps are listed in Appendix 2, where the account of drying, impregnation and autoradiography are indicated for each pieces sample.

Table III. Faul breccia pieces - weights, sample priority, experiment codes and ^{14}C-MMA tracer activities. Porosity values measured with water saturation method [1,2]

	weight (g)	priority	tracer activity (mCi/ml)	porosity with water saturation (vol-%)
A				
#22 KI0025F02:66.7m	11.95	1	25	1.5
#20 KI0023B:69.9m	10.58	3	25	0.7
B				
#22 KI0025F02:66.7m	1.46	1	0.7	
#20 KI0023B:69.9m	5.01	3	0.7	

2.3 Wall rock samples

"Wall rock samples" were ordinary core samples, 51 mm or 41 mm in diameter, with exposed natural fracture surfaces. A total of 6 core samples were impregnated with ^{14}C-MMA. The wall rock samples were dried using a maximum temperature of 90 °C. The used tracer activity was 25 µCi/ml. The codes, the lenghts and the diameters of each wall rock sample are shown in Table IV. The samples are listed in the order of the assigned priority.

The sample structure #22 in KI0025F02:66.7m had two fracture surfaces (A and B). The porosity values of the intercept structure #23 in KI0025F02:56.8m were determined with water saturation method [1,2] and these values are compared to the values of ^{14}C-PMMA method. Due to improper intrusion of MMA into the rock matrices, part of the once impregnated wall rock samples were impregnated yet another time. A detailed account of

drying temperatures, drying and impregnation times and all the autoradiographs from different sawn rock surfaces are listed in Appendix 3.

Table IV. Wall rock - codes, diameters and lengths of samples.

feature id	intercept (m)	diameter (mm)	length (mm)
#22	**KI0025F02:66.7m**	51	50
#23	**KI0025F03:56.8m**	51	20
#20	**KI0023B:69.9m**	51	100
#21	**KI0023F:71.1m**	51	80
#20	**KI0025F02:74.6m**	51	55
#20	**KA2563:188.7m**	41	85

2.4. The ^{14}C-PMMA method

2.4.1 General

The ^{14}C-PMMA method involves impregnation of centimetric scale rock cores with ^{14}C labelled methylmethacrylate (^{14}C-MMA) in a vacuum, irradiation polymerisation, autoradiography and optical densitometry with digital image processing techniques [3-7]. Impregnation with the labelled low-molecular-weight and low-viscosity monomer ^{14}C-MMA, which wets the silicate surfaces well and can be fixed by polymerisation, provides information on the accessible pore space in crystalline rock that cannot be obtained with other methods. In the work the ^{3}H labelled methylmethacrylate was also used to provide porosity information of fault breccia fragments.

Total porosity is calculated using 2D autoradiographs of the sawn rock surfaces. The geometry of porous regions is then visualised. The preconditions for applying this method are: (i) known local bulk density; (ii) presence of only two phases; minerals and PMMA; and (iii) homogeneous distribution of pores and minerals below the limit of lateral resolution of autoradiography. The PMMA procedure is presented in Figure 2-1 showing experimental part A and analysis tools B.

A

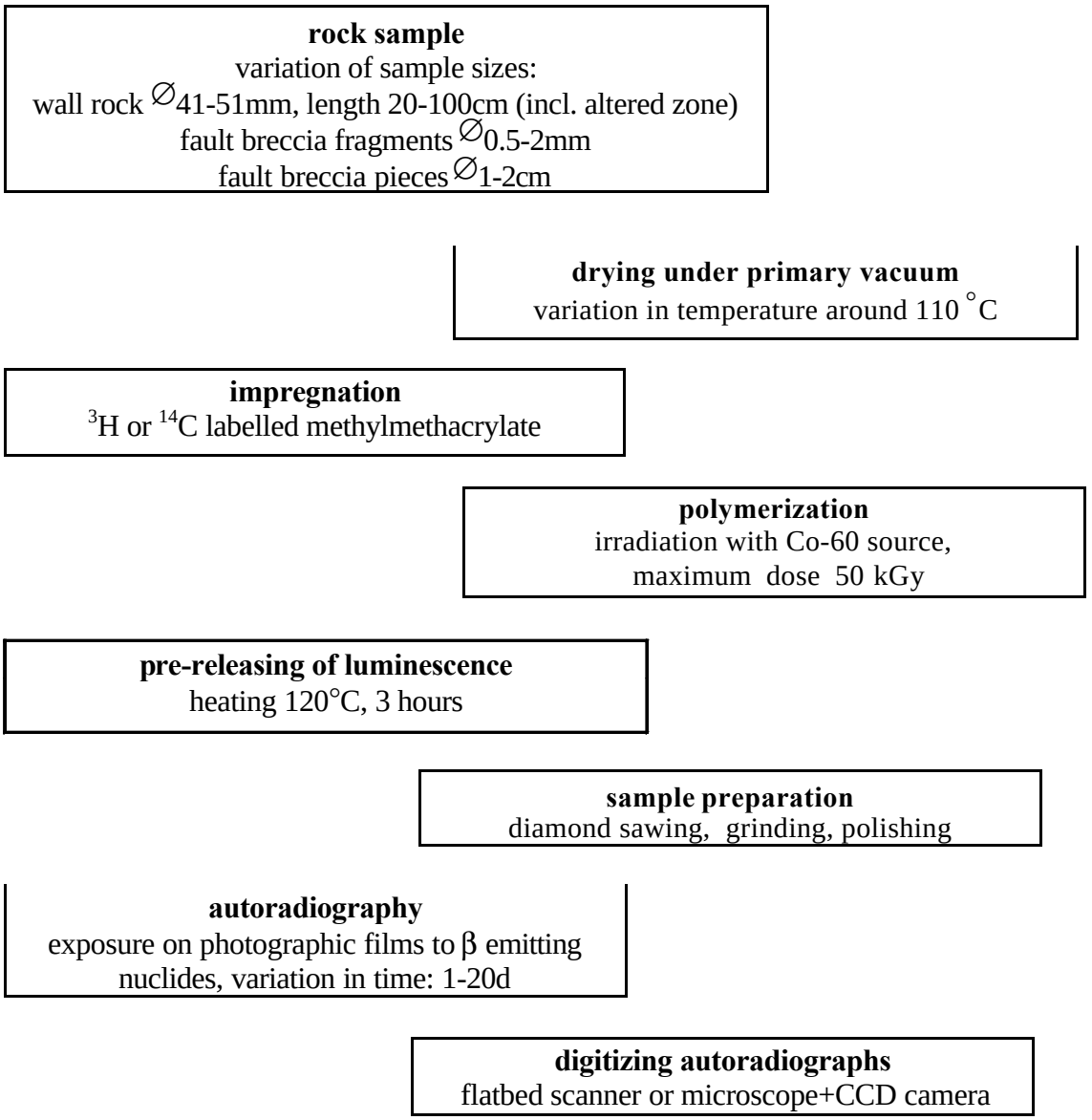

B

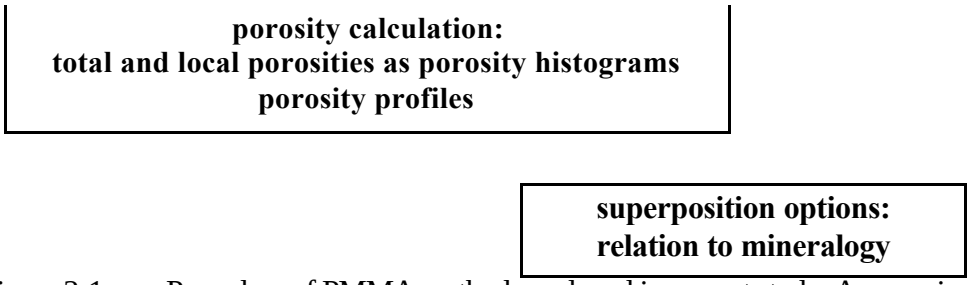

Figure 2-1 Procedure of PMMA method employed in current study. A=experimental part, B=digital image analysis

2.4.2 Properties of the ^{14}C-MMA and the ^{3}H-MMA tracers

Methylmethacrylate (MMA) is a monomer with very low viscosity, 0.00584 P (20°C) [8], while the viscosity of water is 0.00895 P (25°C) [9]. Because its contact angle on silicate surfaces is low, impregnation of bulk rock specimens is rapid and depends on existing pore apertures. The MMA molecule is small (mol.weight 100.1). It has non-electrolytic properties and only low polarity, the polarity of the ester being considerably lower than that of water, and it behaves in the rock matrix as a non-sorbing tracer. The low β energy of the Carbon-14 isotope, max 150 keV, is convenient for autoradiographic measurements.

The monomer used was ^{14}C-labelled MMA with a specific activity of 2–5 mCi/g and a total activity of 50 mCi. Its radiochemical purity was >95 %. In this study the dilution of the tracer was around 25 μCi/ml. The tracer activity used was determined with liquid scintillation counting (Rackbeta 280). The calibration sources were prepared by diluting the ^{14}C-MMA with inactive MMA. The activities ranged from 0.0125 μCi/ml to 5 μCi/ml.

^{3}H labelled MMA was applied to the experiments due to the extremely low beta energy of the tritium isotope, maximum energy of 18 keV. Total amount of methyl-[2,3-3H] methacrylate was 185 000 MBq, specific activity being 3 mCi/ml and radiochemical purity >95 %. 100 ppm hydroquinone was used for stabilization. The range of the 18 keV beta rays in the rock matrix of 2.7 g/cm^3 density is 2.5 μm [10]. The spatial resolution of the autradiographs using ^{3}H-PMMA is better than that of ^{14}C-PMMA due to the lower energy, but on the other hand a higher specific activity of ^{3}H is needed to provide an autoradiographic image, which is restricting the use of tritium labelled methylmethacrylate. Another drawback is that even the diluted ^{3}H labelled methylmethacrylate autopolymerizes easily and restrict the use of ^{3}H labelled MMA over longer times. The organic reaction for labelling MMA with ^{3}H is a more demanding procedure than the reaction for labelling MMA with ^{14}C.

2.4.3 Drying, impregnation with ^{14}C-MMA and polymerization of samples

Samples were vacuum dried in aluminium chambers for 2-6 days at a maximum temperature of 120°C for samples of fragments and pieces and at a maximum temperature of 90°C for wall rock samples. After drying the samples were cooled to 18°C. For ^{14}C-MMA impregnation, the tracer was put into a 50 ml reservoir and transferred under vacuum to the impregnation chamber. The fragments were dried and impregnated in the glass vials (volume of 10 ml). Slow transfer of the monomer ensures degassing of the monomer and infiltration without vapor. The impregnation time varied between 1-10 days. After impregnation the samples were irradiated with gamma rays from a Co-60 source, in order to polymerise the monomer in the rock matrix; the required dose was 50 kGy (5 Mrad). The fragments were irradiated with a Hot Spot type gamma source. The fragments and the pieces were irradiated under radioactive ^{3}H- and ^{14}C-MMA; fragments in the glass vials and pieces in the polyethylene vials to avoid the outdiffusion of tracer before it is polymerized. Due to the small size of these sample types the outdiffusion of tracer would significantly prevent the measurement. The wall rock samples were irradiated under ^{14}C-MMA saturated water in polyethylene vials.

2.4.4 Autoradiography

Irradiation of the rocks with Co-60 causes strong thermoluminescence of K-feldspar and other major rock-forming minerals, which exposes autoradiographic film. To avoid this, the thermoluminescence was released by heating the samples to 120°C for 3 hours before sawing. Mylar foil with aluminium coating was placed on top of the film to shield it from the rest of the emissions in the case of ^{14}C-PMMA impregnated samples. The foil was not used in the case of ^{3}H-PMMA samples, because the low beta energy of tritium.

The heated samples were sawn into pieces. The partitioning of each sample is illustrated in pictures taken with the digital camera (see chapter 3). The sawn rock surfaces of ^{14}C-PMMA impregnated samples were exposed on Kodak BioMax MS autoradiographic film. The ^{3}H-PMMA impregnated sawn or grinded fragment samples were exposed on Hyperfilm ^{3}H, from Amersham. The films are high-performance autoradiographic films for ^{14}C and for ^{3}H, respectively. The resolution of the β film is a few μm. The final resolution

depends on the roughness of the sawn surface, which control the width of interlayer space between the film and the rock. The penetration range of the 150 keV beta particles of ^{14}C or 18 keV beta particles of ^{3}H in dense rock matrix affects strongly on the resolution of autoradiographs. As to the range, the rock samples used were infinite in thickness. The beta absorption correction is obtained from the ratio of the densities of rock and polymethylmethacrylate and its effects on the qualitative porosity calculation.

With the tracer activities and the autoradiographic films employed here, the exposure times for samples ranged from 1 to 2 days for ^{3}H-PMMA fragment samples and 3 to 20 days for ^{14}C-PMMA samples

2.5 Digital image analysis of ^{14}C-PMMA and ^{3}H-PMMA autoradiographs

2.5.1 Calculation of porosity

Interpretation of the results is based on digital image analysis of autoradiographs. Digital image analysis starts by dividing the autoradiograph into area units called pixels. The autoradiographs were scanned using 400 dpi resolution (pixel size of 62 x 62 μm) for the quantitative analysis. Basically all the intensities of the subdomains (pixels) were converted into corresponding optical densities, which in turn were converted into activities with the help of the calibration curves measured for each exposure. Finally, the activities were converted to corresponding porosities. In principle, the interpretation is based on studying the abundance of tracer in each subdomain. The program Mankeli calculates the porosities from the autoradiographs based on the equations interpreted in the following chapters. The program is implemented using Matlab.

2.5.2 Intensity and optical density

Since the response of the image source (table scanner or CCD camera) and the amplifier of the digital image analyser are linear, the digitised grey levels of the film can be handled as intensities. Optical densities, which according to Lambert & Beer's law are concentration proportional, are derived from the intensities:

$$D = \log\left(\frac{I_0}{I}\right) \qquad 2\text{-}1$$

where D is the optical density, I_0 is the intensity of the background and I is the intensity of the sample. It can be seen that as the intensity decreases, the optical density increases.

2.5.3 Activity and optical density

A conversion function is needed to relate the optical densities measured to corresponding activities. ^{14}C-PMMA standards (tracer diluted with inactive MMA) having specific activities between 462 and 185 000 Bq/ml have been used to establish the calibration function. The following calibration curve was used:

$$D = D_{\max}(1\text{-}e^{-kA}) \qquad 2\text{-}2$$

where D_{max} is the maximum optical density, k is a fitting parameter, and A is the specific activity. Solving A from the Eq. 1-2 gives:

$$A = -k^{-1}\ln(1 - D / D_{\max}) \qquad 2\text{-}3$$

2.5.4 Porosity

The local porosity ε of the sample was simply obtained from the abundance of the tracer (assuming constant tracer concentration in the PMMA, the higher the abundance of the tracer, the higher the local porosity):

$$e = b(A / A_0) \qquad 2\text{-}4$$

where A_0 is the specific activity of the tracer used to impregnate the rock matrix, and β is the β-absorption correction factor. The absorption of β radiation in a substance depends

roughly linearly on the density of the substance. Therefore factor β can be approximated from:

$$\beta = \rho_s / \rho_0 \qquad 2\text{-}5$$

where ρ_s is the density of the sample and ρ_0 is the density of pure PMMA (1.18 g/cm^3). In the interpretation the sample is assumed to consist of rock material and pores (containing PMMA), and therefore ρ_s can be expressed as:

$$\rho_s = \varepsilon\rho_0 + (1-\varepsilon)\rho_r \qquad 2\text{-}6$$

where ρ_r is the density of mineral grains. In the practice of bulk measurements the average density of the rock sample is used. Using Eqs. 2-5 and 2-6 in Eq. 2-4, the porosity and the activity relationship can be solved as:

$$\varepsilon = \frac{\frac{\rho_r}{\rho_0}}{1+\left(\frac{\rho_r}{\rho_0}-1\right)\frac{A}{A_0}}\frac{A}{A_0} \qquad 2\text{-}7$$

where A is the specific activity of individual pixel and A_0 is the specific activity of the tracer. The porosity of each individual pixel n in the autoradiogram is calculated according to equations 2-3 and 2-7. The porosity histogram gives the relative frequency of regions of individual porosities. The total porosity is obtained from the porosity distribution by taking the weighted average:

$$\varepsilon_{tot} = \frac{\sum_n Area_n \varepsilon_n}{\sum_n Area_n} \qquad 2\text{-}8$$

where $Area_n$ is the area of pixel n, and ε_n is the local porosity of pixel n.

The amount of tracer in the sample, and the volumetric porosity, can thus be derived from the blackening of the film caused by the radiation emitted from the plane surface of the rock section. If the pore sizes are well below the resolution of the autoradiography, the major fraction of the beta radiation emitted is attenuated by existense of silicate. The tracer can thus be considered diluted by existence of silicate. For the ^{14}C-PMMA method to be used, the bulk density must be known; there must be only two phases (mineral and PMMA), and pores and minerals must be homogeneously distributed below the limit of the lateral resolution of the autoradiography. The bulk densities were taken in the work from references [1] and [2].

The porosity profiles were measured from the autoradiographs taken from the surfaces of sawn rock samples sawn perpendicular to the fracture surfaces of wall rock sample. Each profile contains several measurements where the thickness of digitally scanned sector varies from 1 to 2 mm. The total porosity profile of each sample is the arithmetic average of the sectors measured. The autoradiograph of wall rock sample structure #20 in KI0025F02:74.6m is shown in Figure 2-2 and the porosity profile of the autoradiograph is shown in Figure 2-3 as an example.

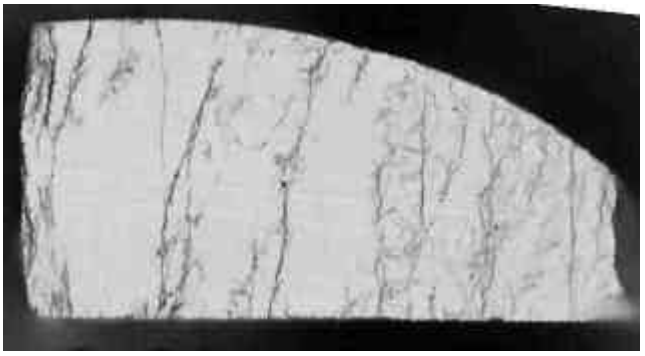

Figure 2-2. Autoradiograph of wall rock sample structure #20 in KI0025F02:74.6m.

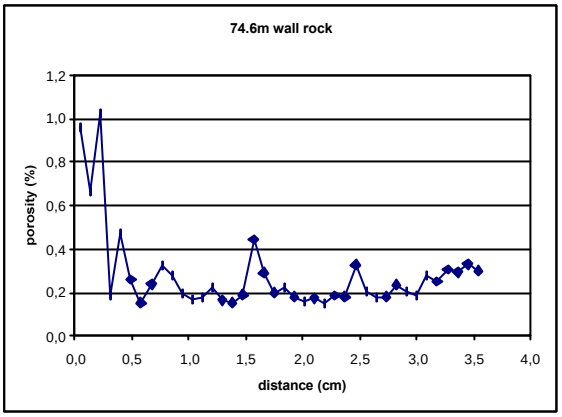

Figure 2-2. Porosity profiles measured from autoradiograph of wall rock sample structure #20 in KI0025F02:76.4m.

2.5.5 Superposition

Digitized autoradiographs was superimposed on digitized images of sawn rock surfaces. This is an effective way to compare rock mineralogy to porosity and microfractures observed on autoradiographs. The autoradiograph and the rock surface are scannned in the same orientation and with the same resolution. Superpositioning is done by moving images in x- and y- direction until they are merged; rotation of the images is not allowed, because it will distort digitized images.

3. RESULTS OF ^{14}C-PMMA IMPREGNATIONS

3.1 Fault breccia fragments

3.1.1 #22 KI0025F02:66.7m

Experimental conditions for fragments of intercept structure #22 in KI0025F02:66.7m are presented in table shown in Appendix 1. All tested fragments (∅ 0.5-1.0 mm; test1 and test2) and part of the prime fragments (∅ 1.0-2.0 mm; test3 and test4) were impregnated with ^{14}C-MMA using different tracer activities; 0.7, 1.2 and 25 µCi/ml. The sample from test3 was cut in two with a low speed diamond saw whereas all other fragments were grinded with grinding paper and with silicon carbide grinding powders. The last part of the prime fragment samples were impregnated with ^{3}H-MMA using the tracer activity of 3 mCi/ml (∅ 1.0-2.0 mm; test5) The photographs of the fragment surfaces and the corresponding autoradiographs are presented in Figs. 3-1 – 3-5.

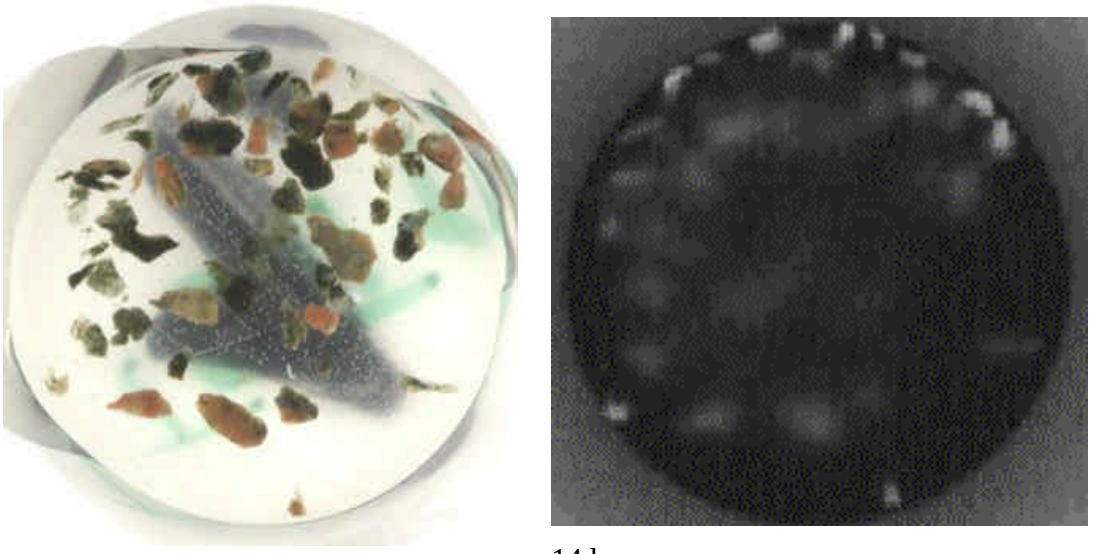

14d exposure

Figure 3-1. Photograph of fragment sample structure #22 in KI0025F02:66.7m 0.5-1.0 mm (left) labelled with ^{14}C-MMA and corresponding autoradiograph (right) (test1).

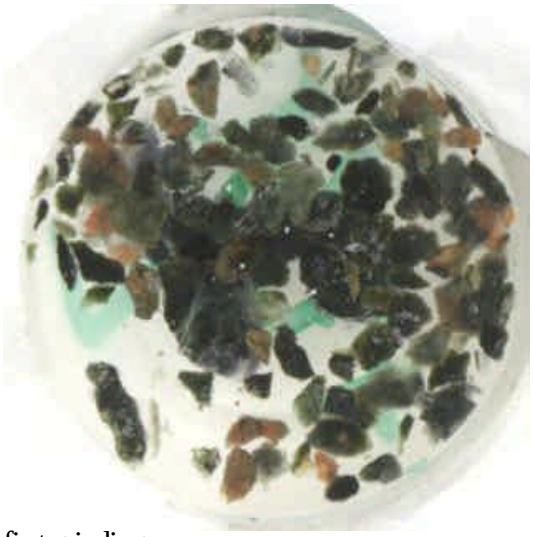

first grinding

14d exposure

second grinding

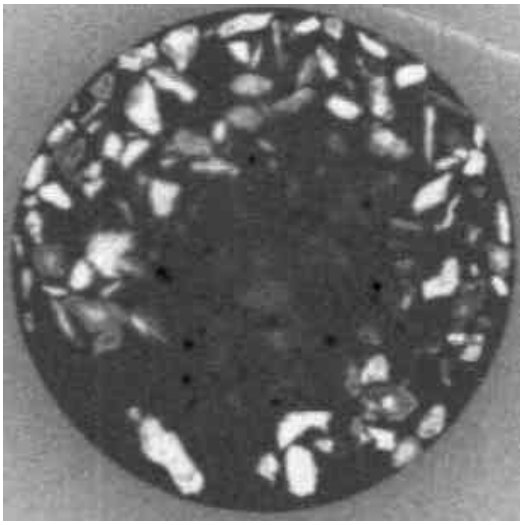

5d exposure

Figure 3-2. Photographs of fragment sample structure #22 in KI0025F02:66.7m 0.5-1.0 mm (left) labelled with ^{14}C-MMA and corresponding autoradiographs (right) (test2).

Test3 I/second grinding

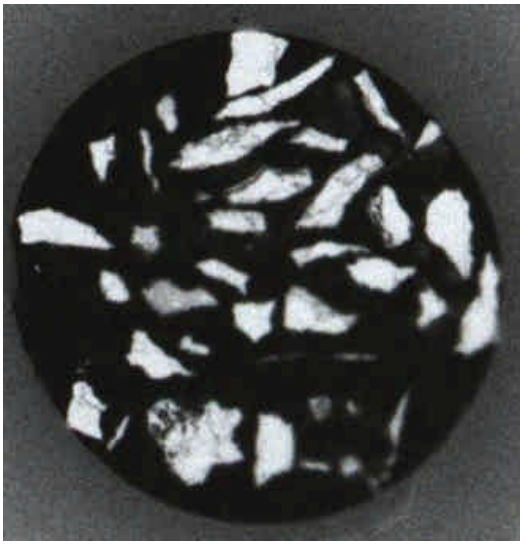

2d exposure

Test3 II/third grinding

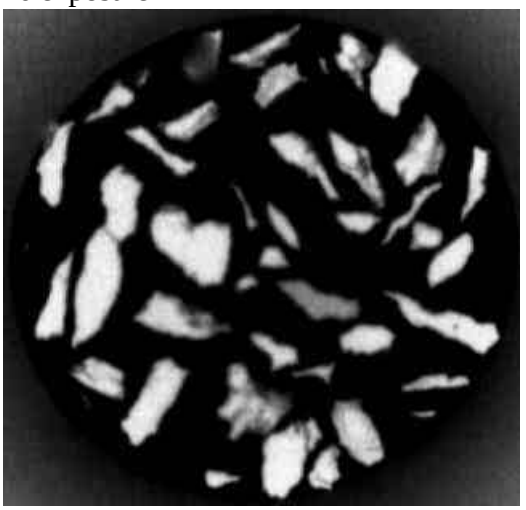

5d exposure

Figure 3-3. Photographs of fragment sample structure #22 in KI0025F02:66.7 m 1-2 mm (left) labelled with ^{14}C-MMA and corresponding autoradiographs (right) of surface II (test3).

Test1 and test2 were done with fragments having a diameter of 0.5-1 mm. The autoradiographs were scanned with 600 dpi. The scanned rock surfaces as well as the corresponding autoradiographs were easily separated, but the details on the autoradiographs were difficult to handle. MMA had intruded into mafic mineral grains while at least some of the feldspars grains were nonporous i.e. MMA did not intrude the fragments. Test3 was done with fragments having diameter of 1-2 mm. Details on the autoradiographs were visualised and cracks and fissures were found in a few MMA impregnated fragments. MMA had intruded into dark minerals. During irradiation the methylmethacrylate

surrounding the fragments had bubbled strongly indicating maybe the need of cooling during irradiation. It might have caused outdiffuion of MMA from the fragments before the polymerization. The rock surfaces for autoradiography proved to be more easier and quicker to employ with a low speed diamond saw than with the time demanding grinding procedure.

^{14}C-labelled MMA tracer having an activity of 25 µCi/ml was used in test4. The best result was achieved from the third grinding of the test4 fragments. Heterogeneous porosity distribution was observed on the autoradiographs of structure #22 in KI0025F02:66.7m fragments. Plenty of cracks and fissures were found in most of the particles. A few porosity measurements were performed (Appendix 4). The porosities varied from 1.3 % up to 11 %. Highest porosities were found in mafic minerals while felsdspars had porosities of a few percent. The porosity distribution of the strongly fissured feldspar grain is presented in Figure 3-5.

second grinding

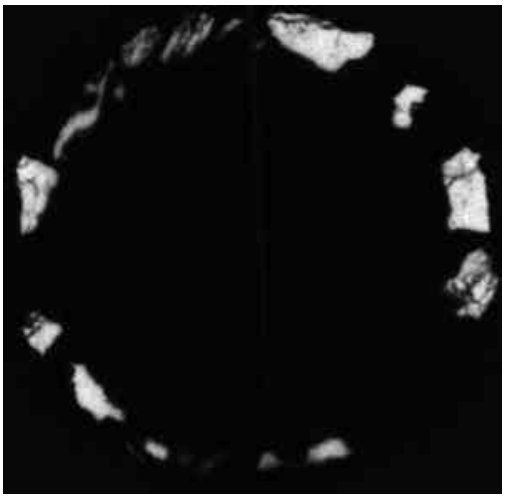

2d exposure

third grinding

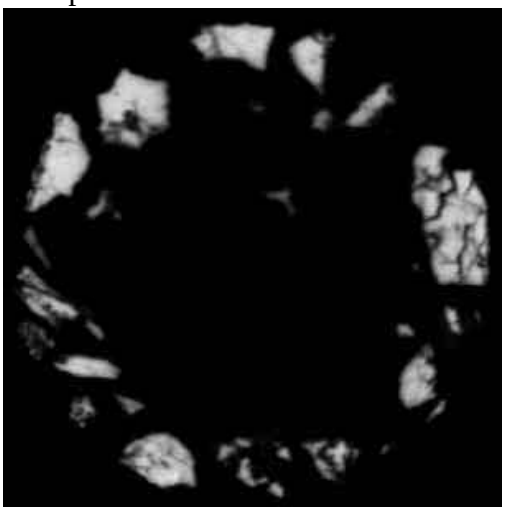

5d exposure

Figure 3-4. Photographs of fragment sample structure #22 in KI0025F02:66.7 m 1-2 mm (left) labelled with ^{14}C-MMA and corresponding autoradiographs (right) (test4).

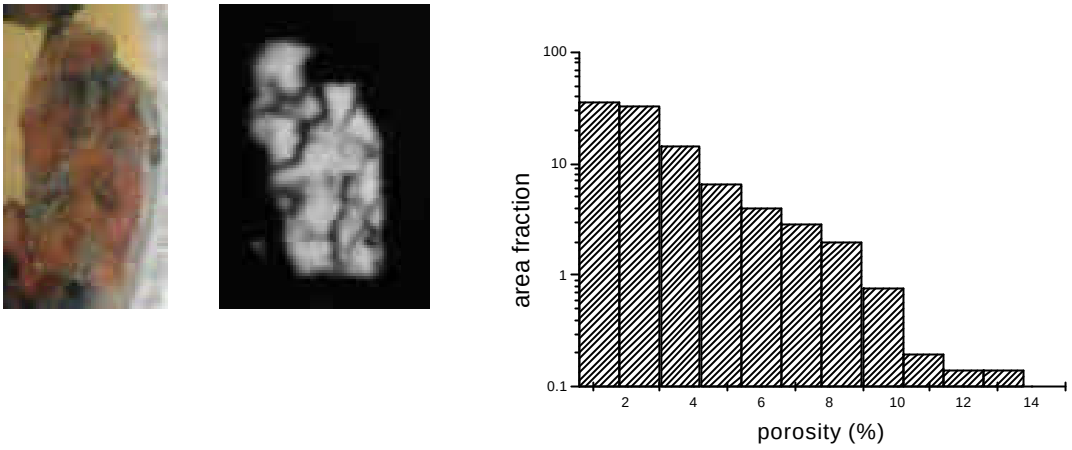

total porosity 2.2 %

Figure 3-5. Porosity histogram for one fragment (3 mm in height) corresponding to a feldspar grain of structure #22 in KI0025F02:66.7 m.

The range of ^{14}C beta particles is 100 µm and there may be equally thin rock fragments in this application. Through these very thin fragments the beta particles of the surrounding radioactive PMMA can penetrate causing erroneous porosity results. The subsequent fragments were impregnated with ^{3}H labelled MMA. The range of ^{3}H beta particles is only 2 to 3 µm, because of the low beta energy (18 keV). Test5 showed qualitatively the same result as test4; some cracks and fissures in the fragments and a few dark minerals showed high porosities, up to 9 % (Appendix 5). The autoradiograph of the test5 fragments was digitized also through stereomicroscope using CCD camera. That way the true resolution (a few microns) of the autoradiograph could be utilized and the detailed qualitative analysis could be performed in much greater detail. The quantitative aspect of the measurement needs more development and testing; the linearity of the microscope+CCD camera needs to be adjusted. The porosity distribution of the mafic mineral grain is presented in Figure 3-7.

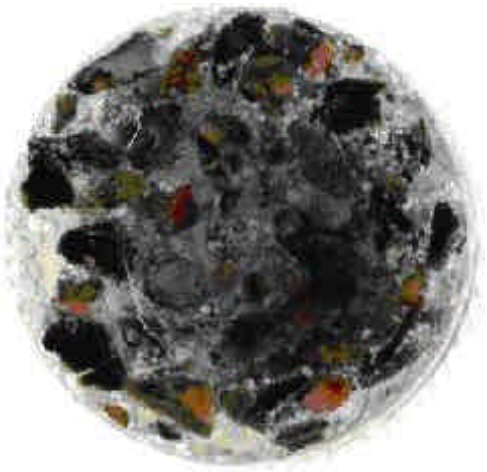

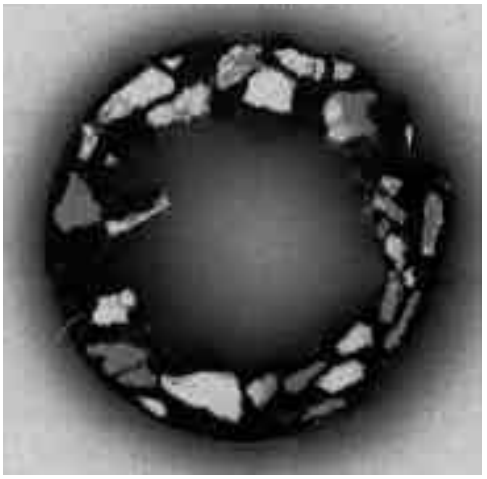

first grinding 2d exposure

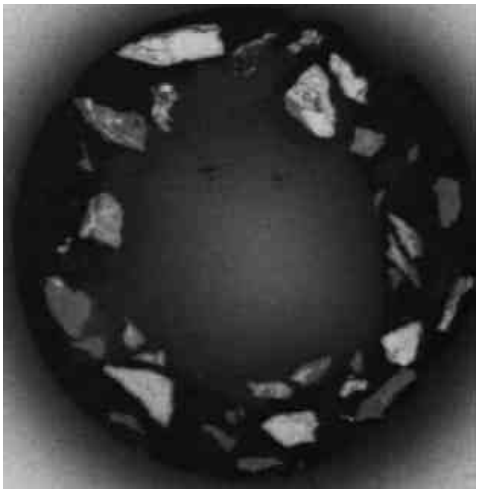

second grinding 2d exposure

Figure 3-6. Photograph of fragment sample structure #22 in KI0025F02:66.7 m 1-2 mm (left) labelled with ^{3}H-MMA and corresponding autoradiograph (right) (test5).

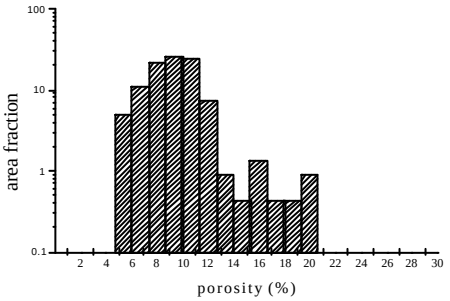

Total porosity of 8%

Figure 3-7. Porosity histogram for one fragment (1.5 mm in width)corresponding to a mafic mineral grain of structure #22 in KI0025F02:66.7 m.

3.1.2 # 20 KI0023B:69.9m

Experimental conditions for the analysis of fragments from intercept structure #20 in KI0023B:69.9m are presented in a table included in Appendix 1. Fragments from this intercept (∅ 0.5-1 mm and ∅ 1.0-2.0 mm) were impregnated with ^{3}H-MMA using a tracer activity of 3 mCi/ml. The photographs of fragment surfaces and corresponding autoradiographs are presented in Figs. 3-8 – 3-9.

first grinding

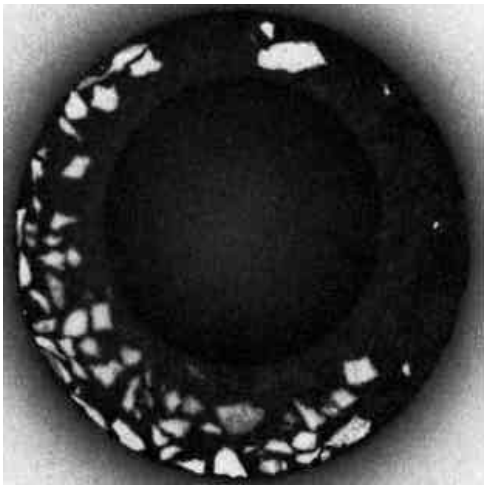

2d exposure

third grinding

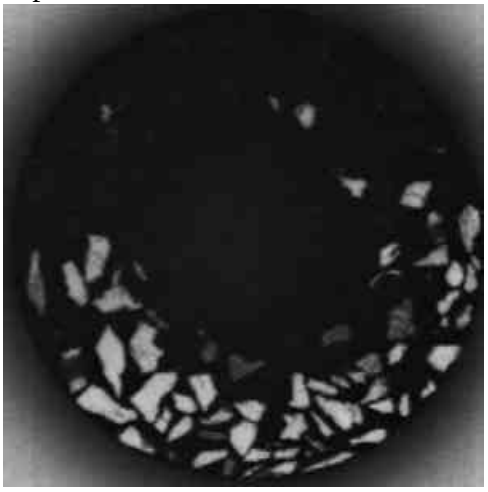

5d exposure

Figure 3-8. Photographs of fragment sample structure #20 in KI0023B:69.9m 0.5-1 mm (left) labelled with ^{3}H-MMA and corresponding autoradiographs (right) (test6).

An effect of few highly porous mineral grains; mainly dark minerals, were found on the autoradiographs of structure #20 in KI0023B:69.9m fragments (0.5-1 mm in diameter, test6). The PMMA which surrounded the fragments was bubbled during irradiation. Diameter of test7 fragaments was 1-2 mm. Again dark mineral grains were found to be porous. The fragments were not microfractured; there were not fissured grains. A few porosity measurements were performed (Appendix 6). The porosities varied from 2 % up to 6 %. The porosity distribution of one plagioclase grain is presented in Figure 3-10.

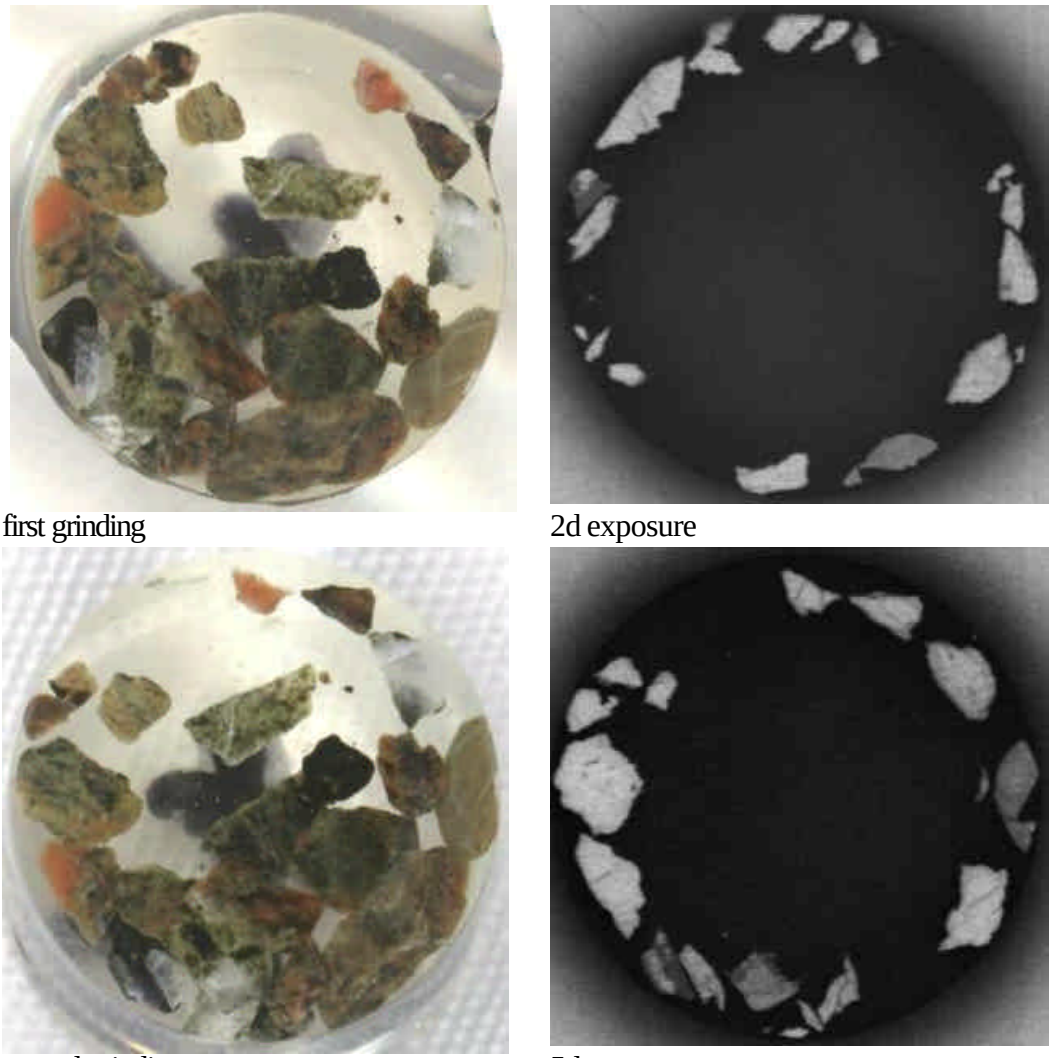

first grinding 2d exposure

second grinding 5d exposure

Figure 3-9. Photographs of fragment sample structure #20 in KI0023B:69.9 m 1-2mm (left) labelled with ^{3}H-MMA and corresponding autoradiographs (right) (test7).

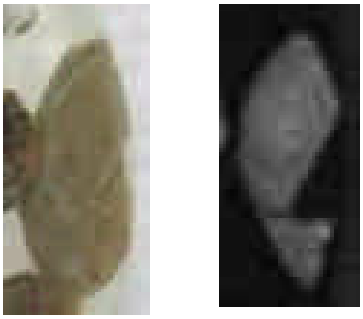

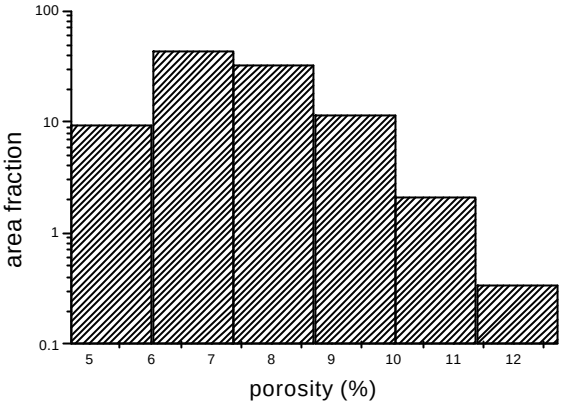

total porosity 7 %

Figure 3-10. Porosity histogram for one fragment (1.5 mm in width)corresponding to a plagioclase grain of structure #22 in KI0025F02:66.7 m.

3.2 Fault breccia pieces

3.2.1 #22 KI0025F02:66.7m

Experimental conditions for sampled pieces from intercept structure #22 in KI0025F02:66.7m are presented in a table in Appendix 2. Two rock pieces (A&B) from intercept structure #22 in KI0025F02:66.7m were impregnated with ^{14}C-MMA. The tracer intruded into both pieces thoroughly. The activities of ^{14}C-PMMA tracer that were used in experiments were 25 µCi/ml for sample A and 0.7 µCi/ml for sample B. The A piece was sawn according to the scheme shown in Figure 3-11.

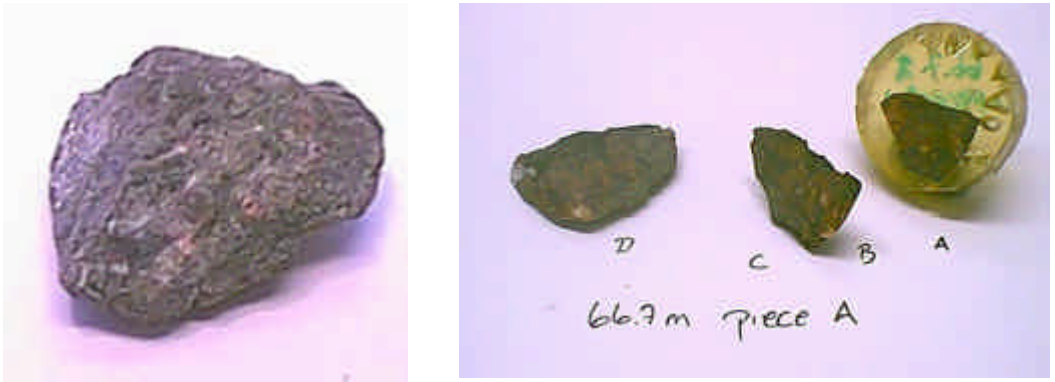

Figure 3-11. Sawings of piece sample A from structure #22 in KI0025F02:66.7m for autoradiography to provide porosity measurements.

The photographs and the corresponding autoradiographs of the piece **A** structure #22 in KI0025F02:66.7m, surfaces B to D, are presented in Figure 3-12. One sawn surface of piece sample A was studied with electron microscopy to evaluate the apertures of microfissures observed on the autoradiograph. The porosity was presented as PMMA porosity histograms for three autoradiographs illustrated in Fig. 3-13.

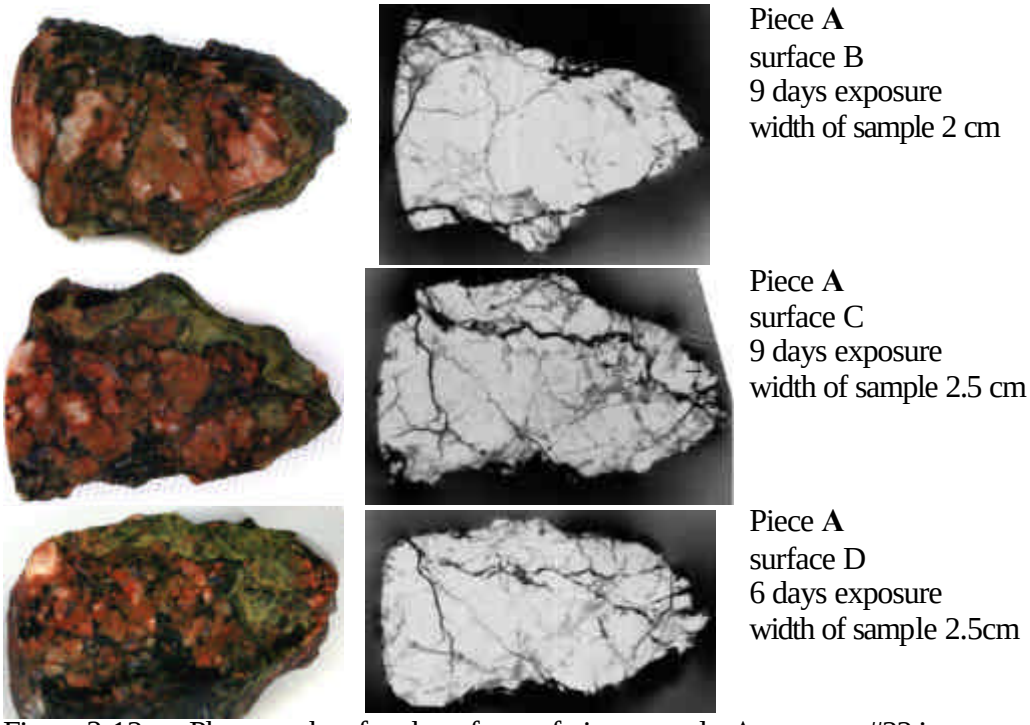

Figure 3-12. Photographs of rock surfaces of piece sample **A** structure #22 in KI0025F02:66.7m, surfaces B, C and D (left), and corresponding autoradiographs (right).

Total porosity of piece A structure #22 in KI0025F02:66.7m varied from 0.4 to 0.8 %. The measurements were done for each sawn rock surface. The highest porosities that were detected were around 8 to 9 %. The apertures of widest fissures that were observed with a scanning electron microscopy were around 10 –15 μm.

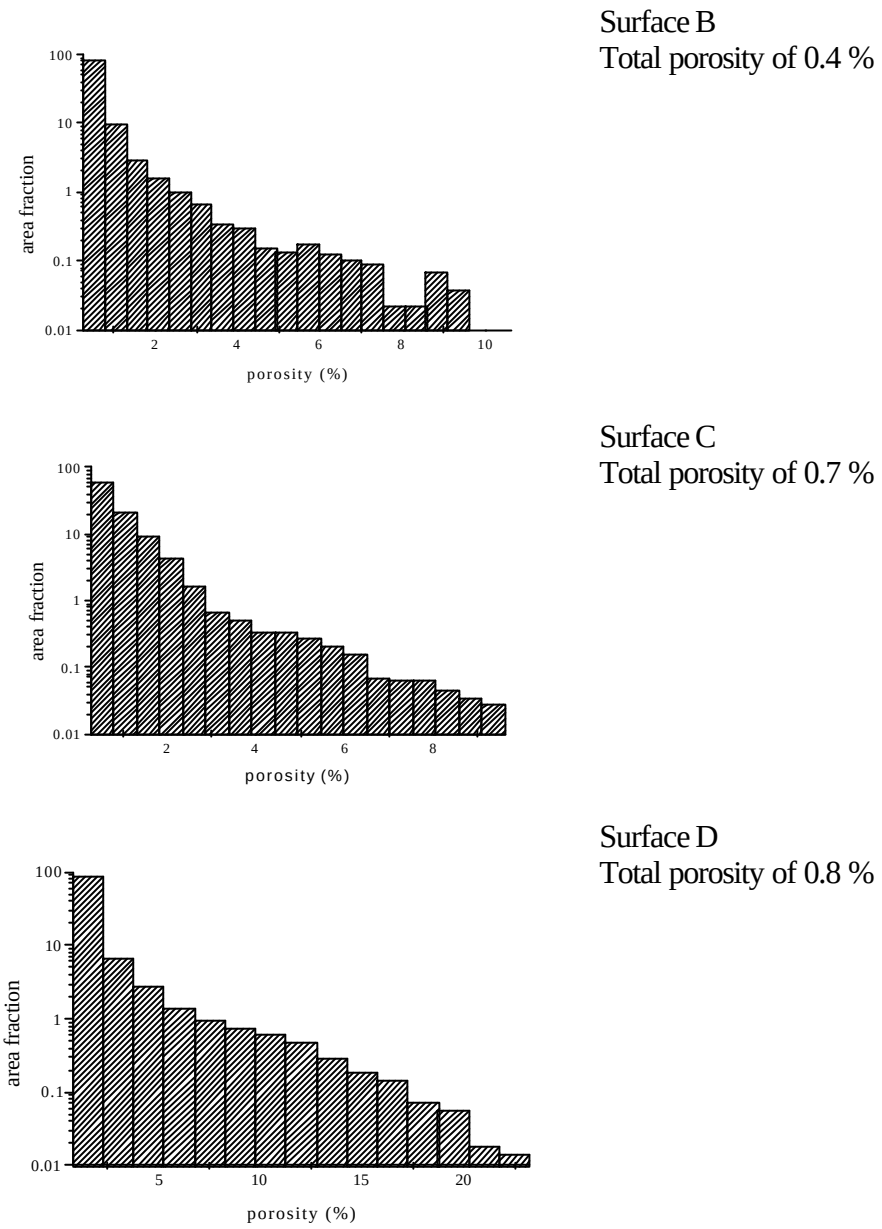

Figure 3-13. Porosity histograms for piece sample A structure #22 in KI0025F02:66.7 m.

The other sample, piece **B** structure #22 in KI0025F02:66.7m was grinded to get a surface for autoradiogaphy. The photograph and corresponding autoradiograph of piece sample **B** are shown in Figure 3-14. MMA had intruded into the piece B. Dark mineral phases were found highly porous >5 % (see arrows in photograph, Fig. 3-14). A few fractures were transsecting the rock sample. A total porosity of 1.4 % was measured with the PMMA method.

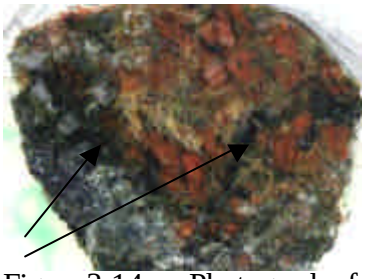

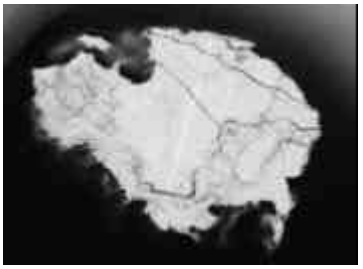

Piece **B**
surface A
12 days exposure
width osf sample 1.5 cm

Figure 3-14. Photograph of rock surface of piece sample B structure #22 in KI0025F02:66.7 m (left) and corresponding autoradiograph (right).

3.2.2 # 20 KI0023B :69.9m

Experimental conditions for the analysis of pieces from the intercept structure #20 in KI0023B:69.9m are presented in a table in Appendix 2. Two pieces samples from structure #20 in KI0023B:69.9 m were impregnated with ^{14}C-MMA. The piece A was thoroughly impregnated with MMA, whereas the piece B was not impregnated with MMA (see Figure 3-18). The piece sample A was sawn according to the partition diagraph shown in Figure 3-15.

Figure 3-15. Sawings of piece sample A from structure #20 in KI0023B:69.9m for autoradiography to provide porosity measurements.

The photographs and the corresponding autoradiographs of piece sample **A** structure #20 in KI0023B:69.9m, surfaces B to F, are presented in Figure 3-16. One sawn surface of piece sample **A** was studied with electron microscopy to evaluate the apertures of microfissures observed on the autoradiograph. The porosity distribution of the rock sample presented as PMMA porosity histograms was provided for two autoradiographs illustrated in Fig. 3-17.

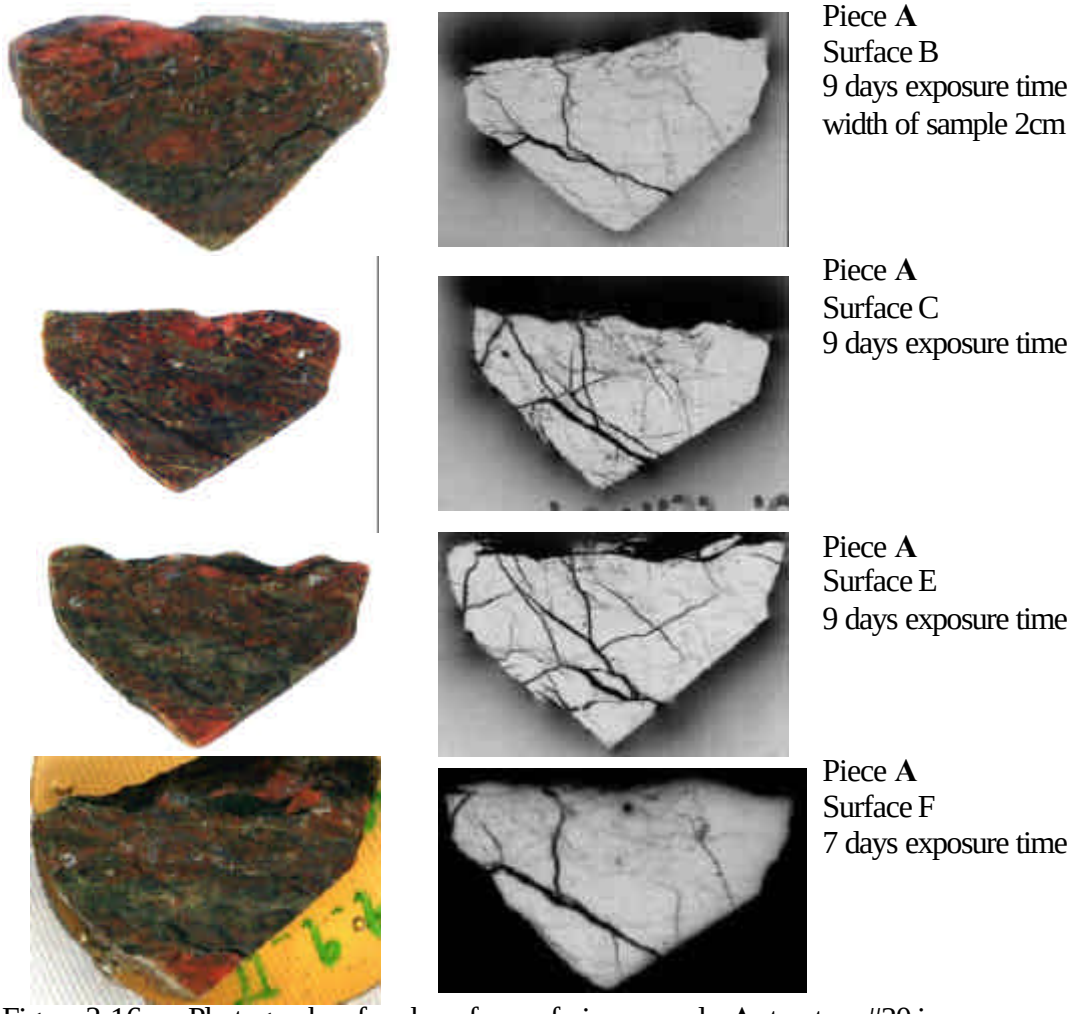

Figure 3-16. Photographs of rock surfaces of piece sample **A** structure #20 in KI0023B:69.9m, surfaces B, C, E and F (left), and corresponding autoradiographs (right).

The total porosity of piece sample A structure #20 in KI0023B:69.9m varied from 0.6 to 0.8 %, the measurements were done on two sawn rock surfaces. The highest porosities that were detected were around 10 %. The apertures of widest fissures that were observed with scanning electron microscopy were around 20 µm.

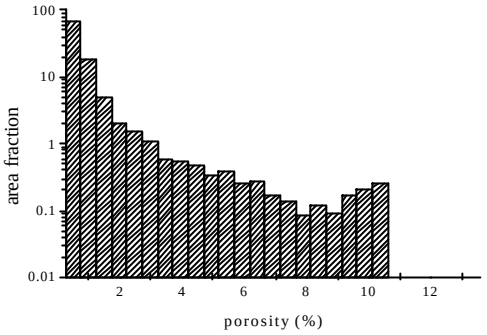

Surface C
Total porosity of 0.8 %

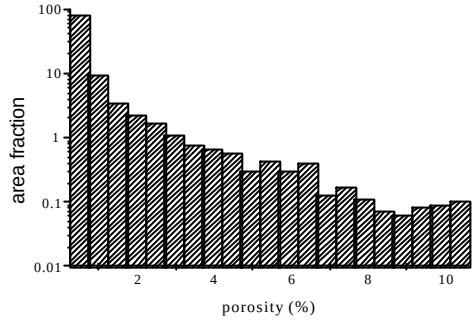

Surface E
Total porosity of 0.6 %

Figure 3-17. Porosity histograms for piece sample A structure #20 in KI0023B:69.9m

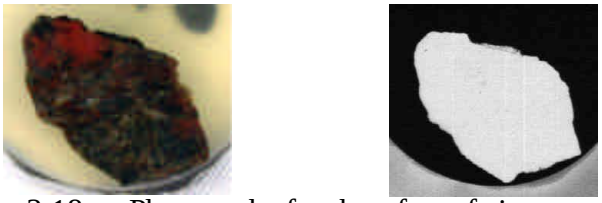

Surface A
12 days exposure

Figure 3-18. Photograph of rock surface of piece sample B structure #20 in KI0023B:69.9m (left) and corresponding autoradiograph (right).

3.3 Wall rock samples

3.3.1 # 22 KI0025F02:66.7m

Experimental conditions for the wall rock sample of intercept structure #22 in KI0025F02:66.7m are presented in a table in Appendix 3. This sample had two separate fracture surfaces A and B. Wall rock sample #22 KI0025F02:66.7 m was not thoroughly impregnated with MMA and one piece of the sample was impregnated twice (66.7 III). In the course of the experiment the sample was sawn according to the partition diagraphs shown in Figures 3-19 and 3-20.

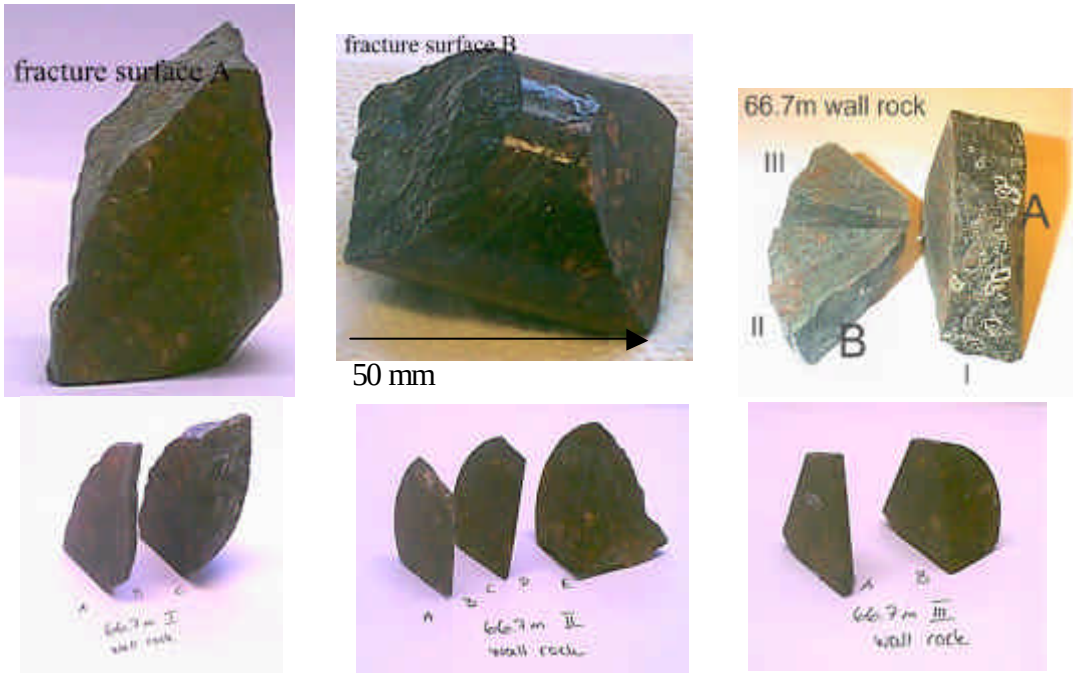

Figure 3-19. Wall rock sample structure #22 in KI0025F02:66.7m sawn perpendicular to fracture surfaces for autoradiography to provide profile measurements.

fracture surface A fracture surface B

Figure 3-20. Wall rock sample structure #22 in KI0025F02:66.7m sawn parallel to fracture surfaces for autoradiography to provide porosity histograms at different depths.

As shown in the autoradiograph of surface I-B of structure #22 in KI0025F02:66.7 in Fig. 3-21 the rock matrix is very dense. MMA has intruded through cracks and fissures and a few mafic mineral phases into the interior of rock matrix, but there is no clear increased porosity zone adjacent to the fracture surfaces. Several further sawings did not reveal any highly porous phases on the autoradiographs taken from sawn surfaces, but more clearly porosity was localized to easily identifiable cracks and fissures (Figs. 3-22 and 3-23).

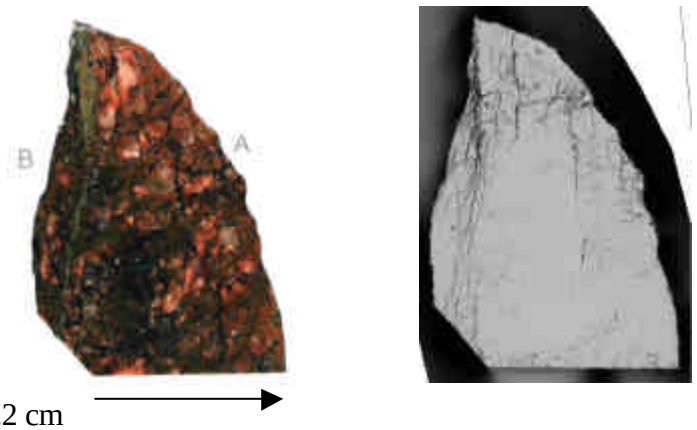

Figure 3-21. Photograph of wall rock sample I-B structure #22 in KI0025F02:66.7m (left) and corresponding autoradiograph (right) (15 d exposure), fracture surfaces A and B marked on the left figure.

2.8 cm

Figure 3-22. Photograph of wall rock sample II-B structure #22 in KI0025F02:66.7m (left) and corresponding autoradiograph (right) (14 d exposure).

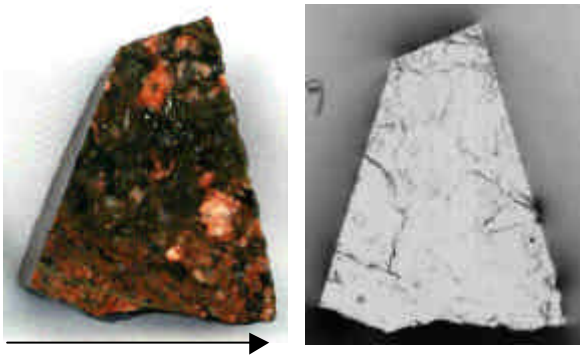

3.0 cm

Figure 3-23. Photograph of wall rock sample III-B structure #22 in KI0025F02:66.7m (left) and corresponding autoradiograph (right) (18 d exposure) -result of 2. impregnation.

One porosity profile measurement was performed and the integrated profile is shown in Fig. 3-24. Over the measured area an increased porosity is observed to a depth of 1 cm from the fracture surface B.

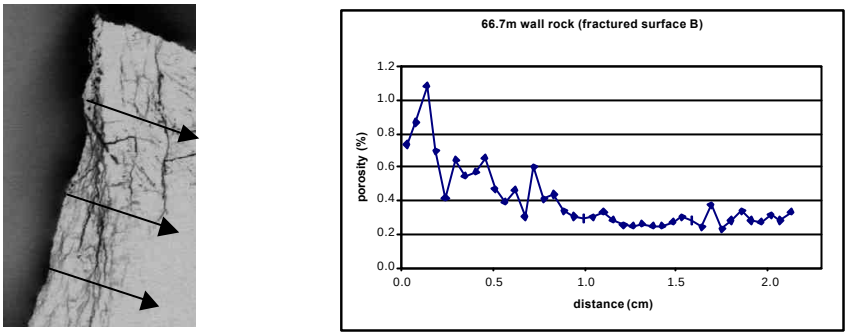

Figure 3-24. Porosity profile of sample I-B structure #22 in KI0025F02:66.7m , measured starting from the fracture surface B.
Scan width was 0.5 mm and total of 4 profiles were measured.

The autoradiographs provided from rock surfaces sawn parallel to the fracture surfaces A and B are shown in Figs. 3-25 and 3-26, respectively. The histograms of measured porosity from the autoradiographs are presented in Figs. 3-27 and 3-28. Total porosities of the measured areas on autoradiographs varied from 0.3 % to 0.6 %. The porosity patterns were heterogeneous and porous phases with up to 6 % porosity were determined at a depth of 10 mm from the fracture surface A, and porosities up to 8 % at a depth of 7.5 mm from the fracture surface B.

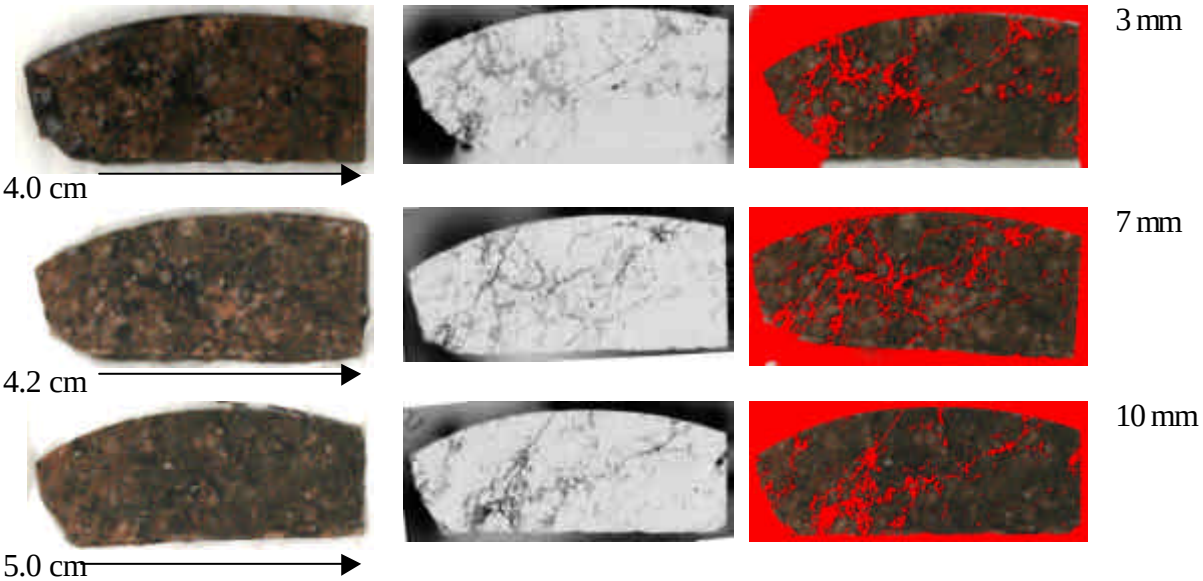

Figure 3-25. Photo images of rock surfaces sawn parallel to fracture surface A (left), corresponding autoradiographs (center, 14 d exposure) and superimposed images (right) showing all porous areas, where MMA has intruded. Depth from the fracture surface is shown in the far right column.

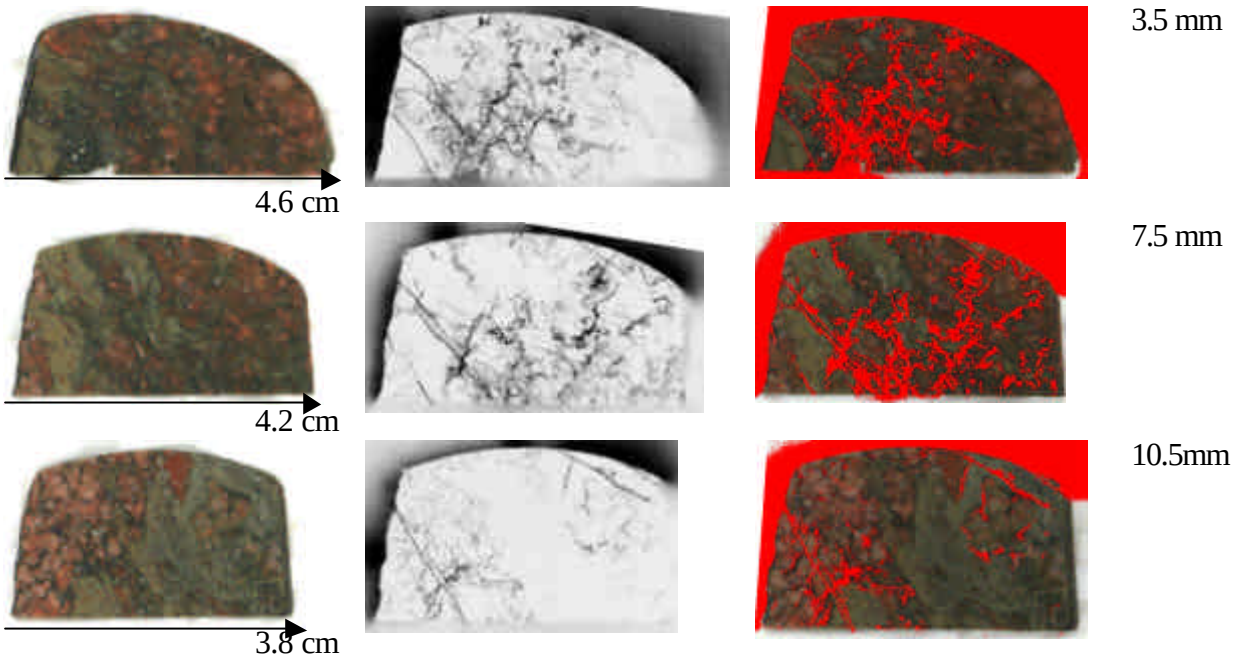

Figure 3-26. Photo images of rock surfaces sawn parallel to fracture surface B (left), corresponding autoradiographs (center, 10 d exposure) and superimposed images (right) showing all porous areas, where MMA has intruded. Depth from the fracture surface is shown in the far right column.

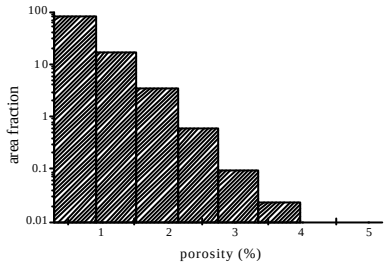

Histogram at a depth of 3 mm from the fracture surface **A**

total porosity of 0.4 %

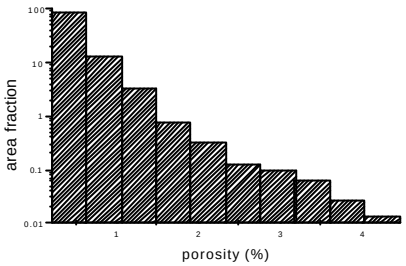

Histogram at a depth of 7 mm from the fracture surface **A**

total porosity of 0.3 %

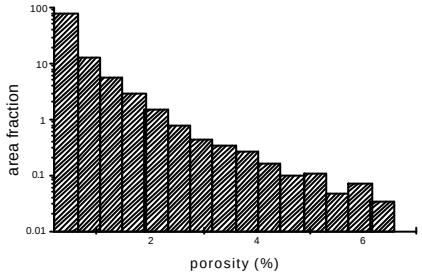

Histogram at a depth of 10 mm from the fracture surface **A**

total porosity of 0.4 %

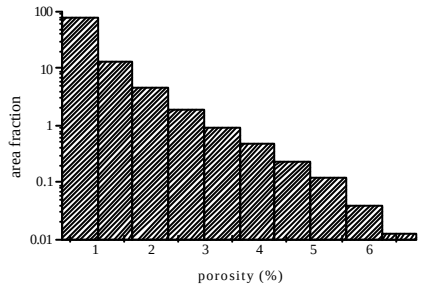

Histogram at a depth of 3.5 mm from the fracture surface **B**

total porosity of 0.6 %

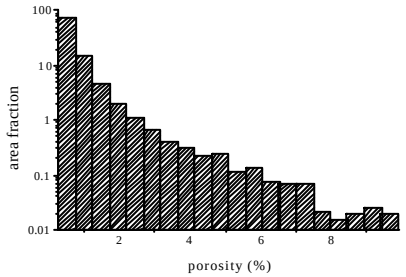

Histogram at a depth of 7.5 mm from the fracture surface **B**

total porosity of 0.5 %

Figure 3-27. Porosity distribution presented as PMMA histograms provided from rock surfaces shown in Figs. 3-23 and 3-24. Surfaces are sawn parallel to fracture surface A and fracture surface B.

3.3.2 # 23 KI0025F03:56.8

Experimental conditions for the wall rock sample from intercept structure #23 in KI0025F03:56.8m are presented in a table in Appendix 3. The wall rock sample structure #23 in KI0025F03:56.8m was not thoroughly impregnated with MMA and one piece of the sample was impregnated twice (56.8 II). As part of the analysis the sample was sawn according to the partition diagraphs shown in Figures 3-28 and 3-29.

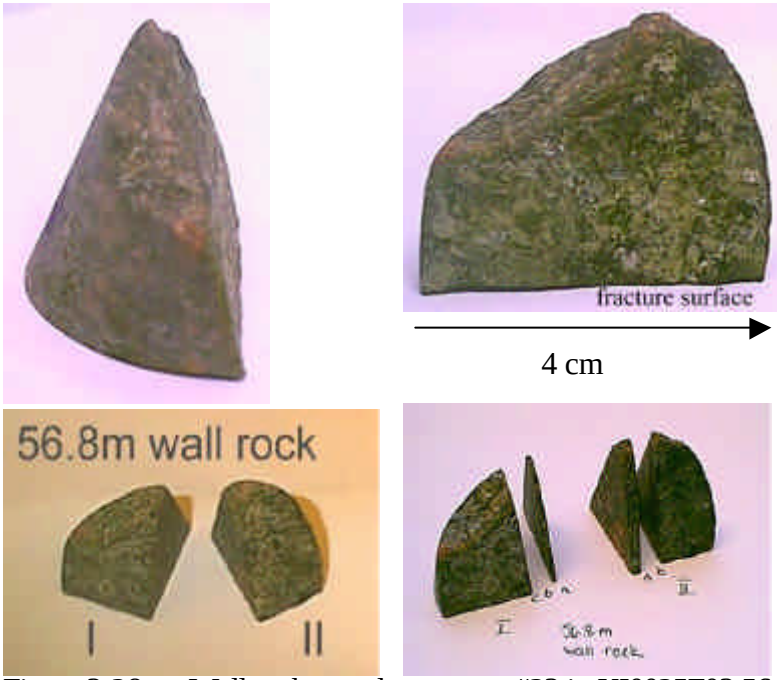

Figure 3-28. Wall rock sample structure #23 in KI0025F03:56.8m sawn perpendicular to fracture surface for autoradiography to provide profile measurements.

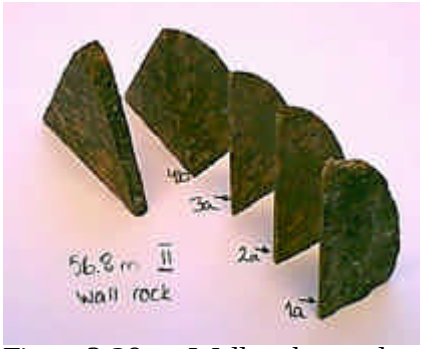

Figure 3-29. Wall rock sample structure #23 in KI0025F03:56.8m sawn parallel to fracture surface for autoradiography to provide porosity histograms at different depths.

As shown in autoradiograph of surface I B structure #23 in KI0025F03:56.8m in Fig. 3-30 MMA has intruded fairly well into the matrix. MMA is found in mafic mineral areas; no appreciable cracks or fissures are found. There is no clear increased porosity zone adjacent to the fracture surface.

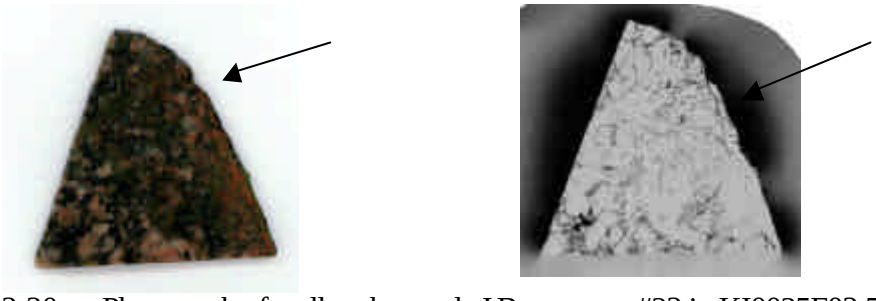

Figure 3-30. Photograph of wall rock sample I B structure #23 in KI0025F03:56.8m (left) and corresponding autoradiograph (right) (15 d exposure). Arrows showing fracture surface.

One example of porosity profile measurement was done and the integrated profile is shown in Fig. 3-31. Only an area extending one or two mm from the fracture surface shows increased porosity.

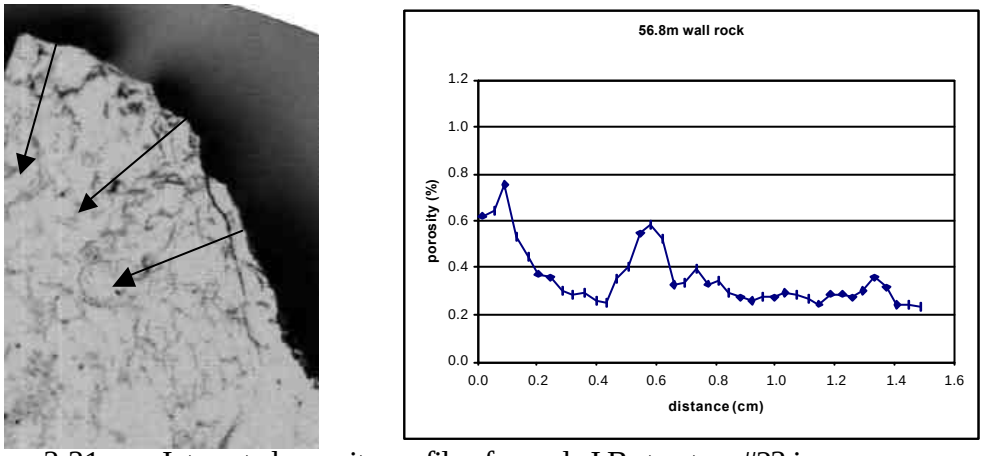

Figure 3-31. Integrated porosity profile of sample I B structure #23 in KI0025F03:56.8m , measured starting from the fracture surface . The scan width was 0.4 mm and total of 3 profiles were measured. Total porosity of rock matrix is 0.3 % with PMMA method.

The second impregnation did not reveal any new porous mineral areas from the wall rock sample structure #23 in KI0025F03:56.8m (Figure 3-32).

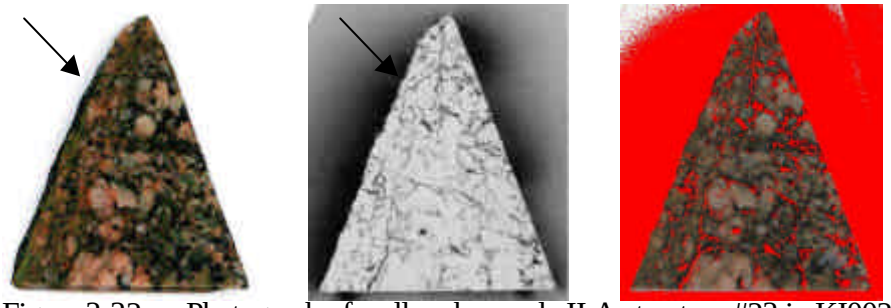

Figure 3-32. Photograph of wall rock sample II A structure #23 in KI0025F03:56.8m (left) and corresponding autoradiograph (center) (18 d exposure) superimposed images (right) showing all porous areas, where MMA has intruded. An arrow showing fracture surface.

The autoradiographs provided from rock surfaces sawn parallel to the fracture surface are shown in Figure 3-33. The measured porosity histograms from two autoradiographs are presented in Figure 3-34. On the autoradiographs it was observed that the porosity pattern of sample structure #23 in KI0025F03:56.8m contains cracks and fissures. Total porosities varied from 0.2 % to 0.5 %. The porosity patterns were heterogeneous and porous phases up to 5 % were determined at a depth of 5 mm from the fracture surface.

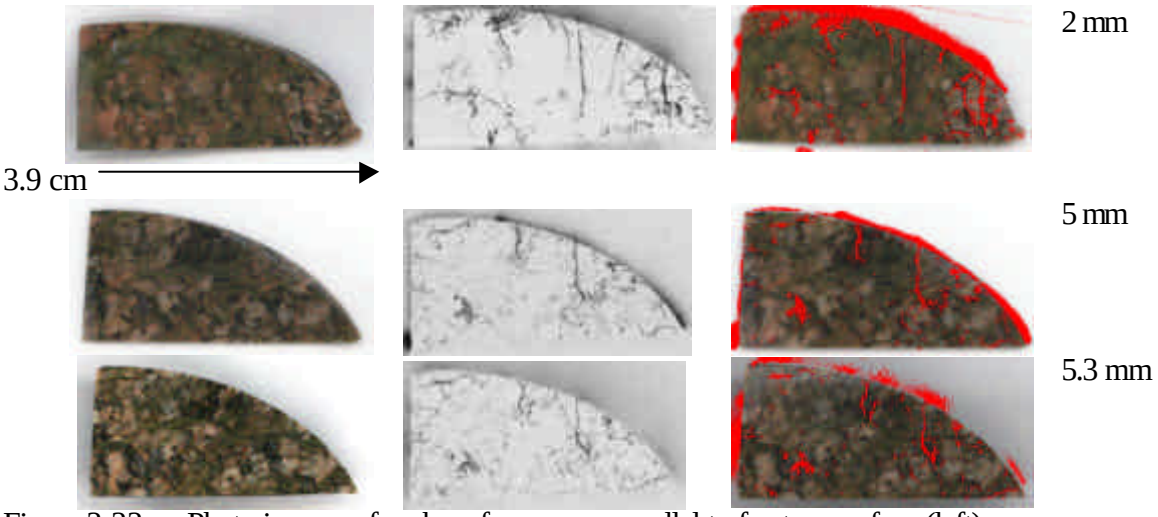

Figure 3-33. Photo images of rock surfaces sawn parallel to fracture surface (left), corresponding autoradiographs (center, 13 d exposure) and superimposed images (right) showing all porous areas, where MMA has intruded. Depth from the fracture surface is shown in the far right column.

2 mm

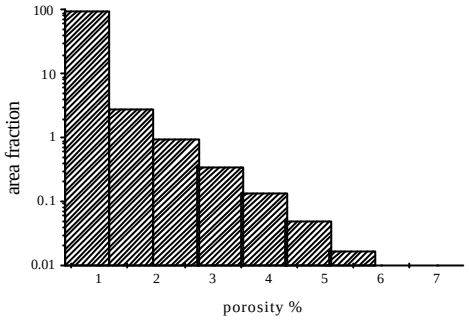

5.3 mm

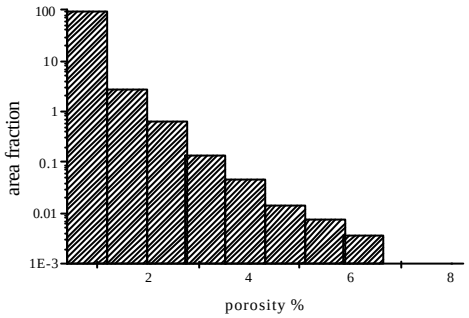

Figure 3-34. Porosity distribution presented as PMMA histograms provided from rock surfaces shown in Figs. 3-33. Depth from the fracture surface is shown in the far right column.

3.3.3 # 20 KI0023B:69.9m

Experimental conditions applicable to the wall rock sample from intercept structure #20 in KI0023B:69.9m are presented in a table in Appendix 3. The wall rock sample structure # 20 in KI0023B:69.9m was not thoroughly impregnated with MMA and half of the sample was impregnated twice (69.9 I). The sample was sawn according to the partition diagraphs shown in Figures 3-35 and 3-36.

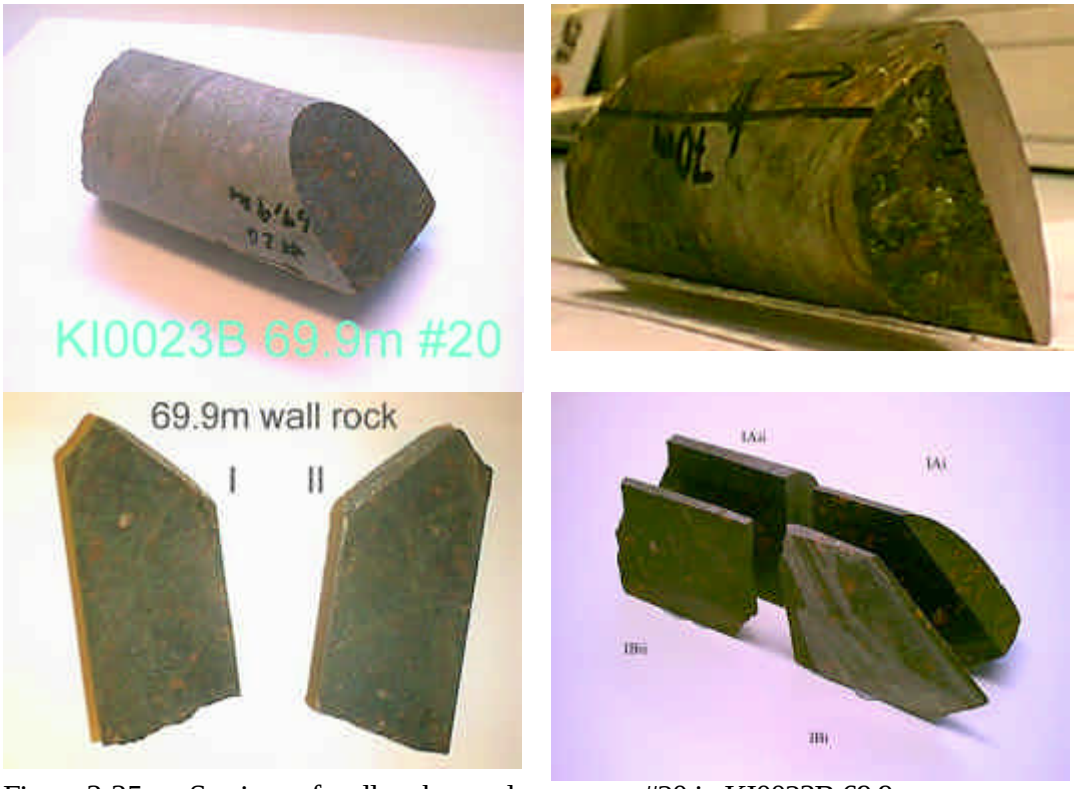

Figure 3-35. Sawings of wall rock sample structure #20 in KI0023B:69.9m; perpendicular to fracture surface for autoradiography to provide profile measurements.

Figure 3-36. Sawings of wall rock sample II structure #20 in KI0023B:69.9m parallel to fracture surface for autoradiography to provide porosity histograms at different depths from fracture surface.

The rock sample is not throughout impregnated with MMA as shown from autoradiograph in Fig. 3-37. The autoradiograph is taken after the second impregnation. MMA has intruded

through cracks and fissures into the rock matrix, but there is no clear increased porosity zone adjacent to the fracture surface. There are a few porous veins trending parallel to the fracture surface at a depth of 1 cm (see an arrow on the autoradiogrtaph in Figure 3-37).

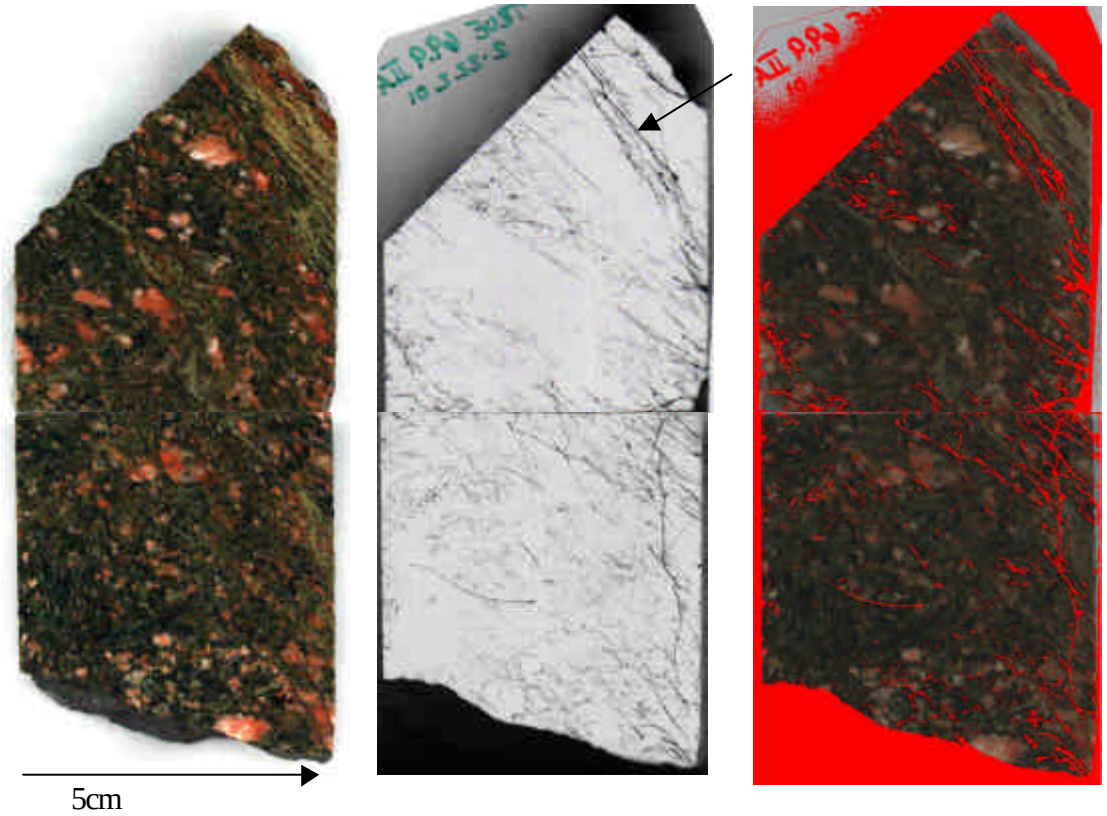

Figure 3-37. Photographs of wall rock samples IAii+IAi structure #20 in KI0023B:69.9m (left) and corresponding autoradiographs (center) (20 d exposure) and superimposed images (right) showing porous areas, where MMA has intruded.

The autoradiographs provided from rock surfaces sawn parallel to the fracture surface are shown in Figure. 3-38. In the autoradiographs it is observed that the porosity pattern of sample structure #20 in KI0023B:69.9m contains cracks and fissures that transsect all mineral phases. The highest porosities measured with the PMMA method were 2 to 3 %, but the total porosities were below 0.1 %. The matrix is very dense and the porosity values measured with the PMMA method should be ragarded as uncertain.

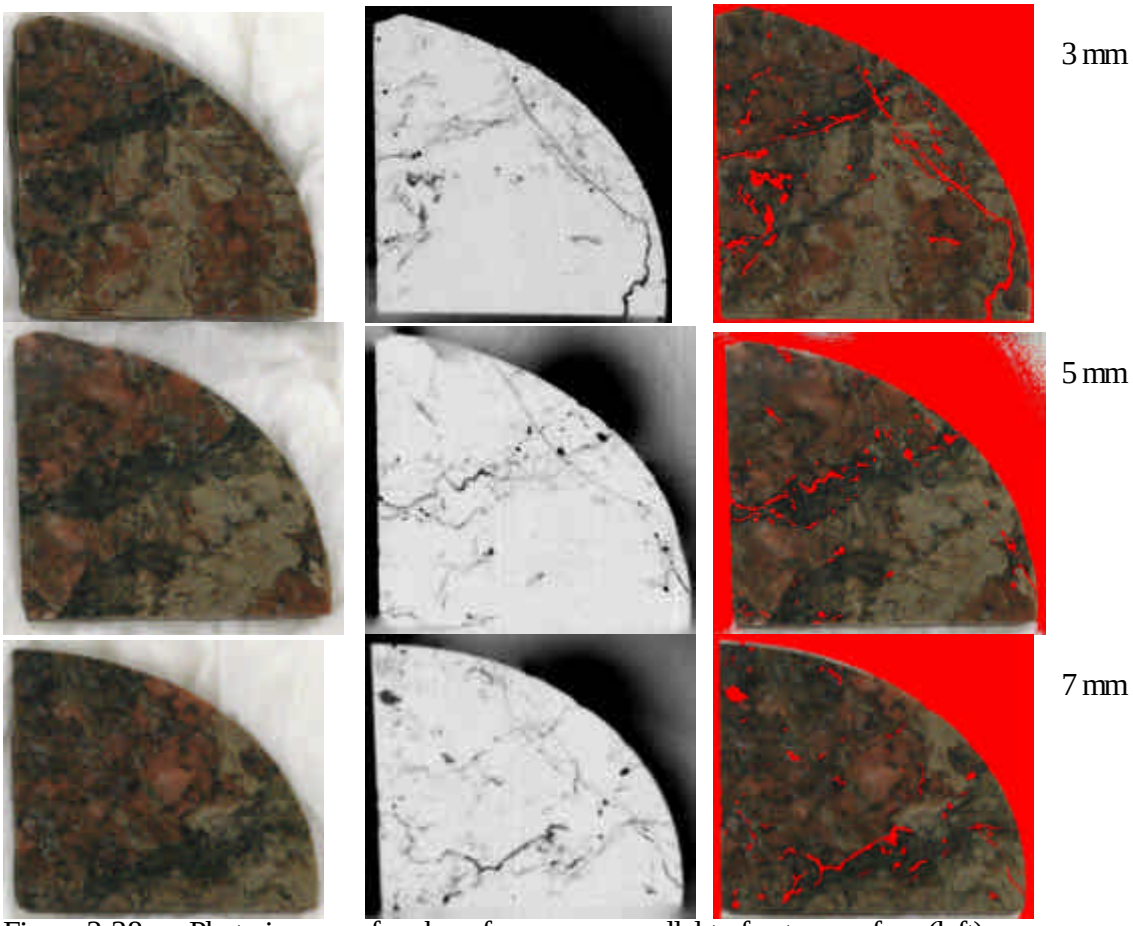

Figure 3-38. Photo images of rock surfaces sawn parallel to fracture surface (left), corresponding autoradiographs (center, 10 d exposure) and superimposed images (right) showing all porous areas, where MMA has intruded. Depth from the fracture surface is shown in the far right column.

3.3.4 #21 KI0023F:71.1m

Experimental conditions for the wall rock sample from intercept structure #21 in KI0023F:71.1m are presented in a table in Appendix 3. This sample was thoroughout impregnated with MMA. The sample was sawn according to the partition diagraphs shown in Figures 3-39 and 3-40.

Figure 3-39. Sawings perpendicular to fracture surface of wall rock sample structure #21 in KI0023F:71.1m for autoradiography to provide profile measurements.

Figure 3-40. Sawings parallel to fracture surface of sample structure #21 in KI0023F:71.1m for autoradiography to provide porosity histograms at different depths. Length of sample is 83 mm.

The photograph of the rock surface of sample structure #21 in KI0023F:71.1m sawn perpendicular to the fracture surface, the corresponding autoradiograph and the superimposed image are presented in Figure 3-41. Porous mineral phases form connected networks of migration pathways. These pathways surround feldspar grains, which are slightly porous. A few cracks and fissures transsect large potassium feldspar phenocrysts. The fracture surface is indicated by an arrow in Fig.3-41. There is no clear increased porosity zone adjacent to the fracture surface found on the autoradiograph. The porosity profile measurement is shown in Fig. 3-42.

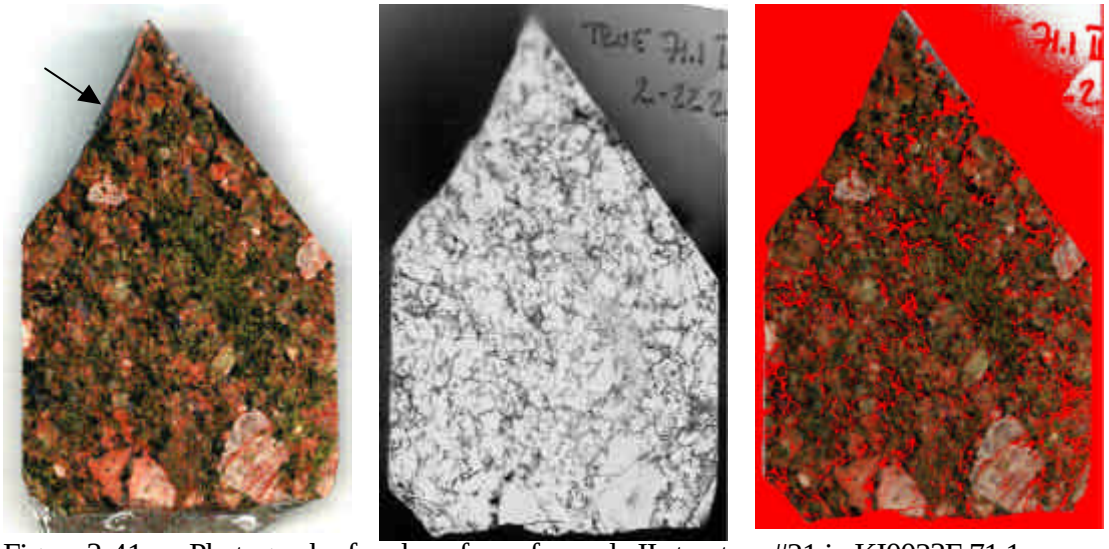

Figure 3-41. Photograph of rock surface of sample II structure #21 in KI0023F:71.1m sawn parallel to fracture surface (left), corresponding autoradiograph (center, 20 d exposure) and superimposed image (right) showing porous areas (>0.5 %), where MMA has intruded.

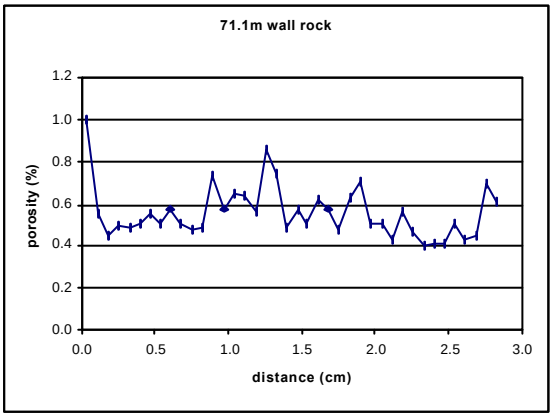

Figure 3-42. The integrated porosity profile of sample II structure #21 in KI0023F:71.1m, measured starting from the fracture surface. The scan width was 0.7 mm and total of 2 profiles were measured.

The porosity distribution was measured from the autoradiograph shown in Fig.3-41 and the histogram is presented in Fig. 3-43. A total porosity of 0.3 % was measured and the highest porosities were ranging from 4 to 5 %.

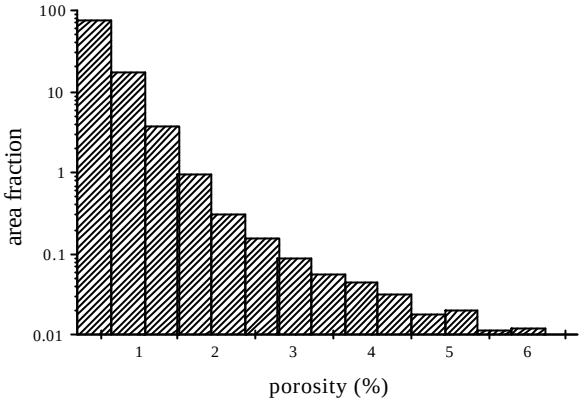

Figure 3-43. Porosity histrogram of sample structure #21 in KI0023F:71.1m. Total porosity of rock matrix is 0.3 % as observed with PMMA method.

The photographs of rock surfaces of sample structure #21 in KI0023F:71.1m sawn parallel to the fracture surface and the corresponding autoradiographs are presented in Figure 3-44. Porous mineral grains and open mineral grain boundaries form connected networks of migration pathways. These pathways surround feldspar grains, which are slightly porous. A few cracks and fissures transsect large potassium feldspar phenocrysts. There is not any increased porosity found adjacent to the fracture surface.

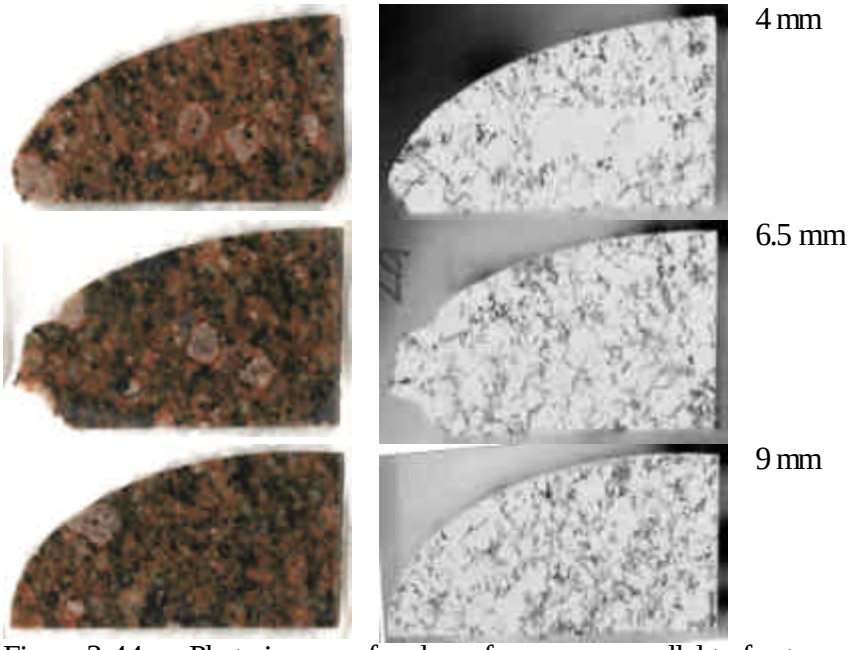

Figure 3-44. Photo images of rock sur faces sawn parallel to fracture surface (left), corresponding autoradiographs (center, 14 d exposure). Depth from the fracture surface is shown in the far right column.

3.3.5 # 20 KI0025F02:74.6m

Experimental conditions for the wall rock sample from intercept structure #20 in KI0025F02:74.6m are presented in a table in Appendix 3. The sample was sawn according to the partition diagraphs shown in Figures 3-45 and 3-46.

Figure 3-45. Wall rock sample structure #20 in KI0025F02:74.6m sawn perpendicular to fracture surface for autoradiography to provide profile measurements.

Figure 3-46. Wall rock sample #20 KI0025F02:74.6m sawn parallel to fracture surface for autoradiography to provide porosity histograms at different depths.

A photograph of the rock sample II structure #20 in KI0025F02:74.6m, the corresponding autoradiograph and the superimposed image showing areas, where MMA has intruded are presented in Fig. 3-47. The zone of increased porosity is a few mm in width as shown in porosity profile in Figure 3-48. The altered mineral phase next to increased porosity zone is nonporous with the PMMA method. The porous veins are localized in dark mineral areas.

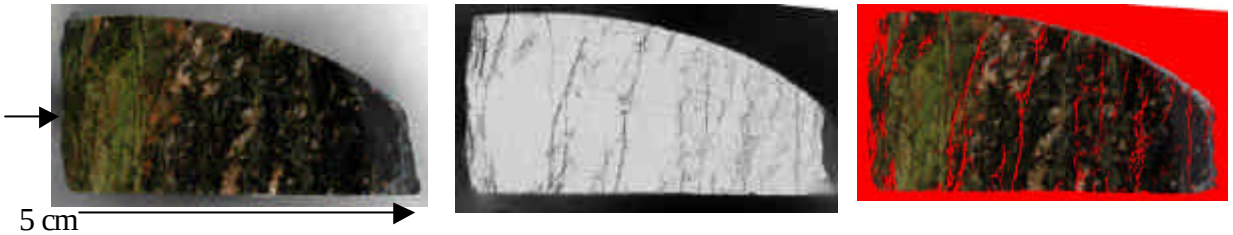

Figure 3-47. Photograph of wall rock sample II structure #20 in KI0025F02:74.6m (left), corresponding autoradiograph (center) (14 d exposure) and superimposed image (right) showing porous areas, where MMA has intruded. An arrow shows the fracture surface.

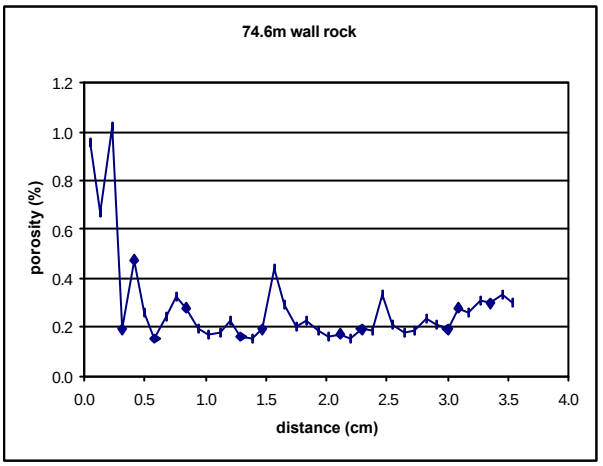

Figure 3-48. The integrated porosity profile of sample II structure #20 in KI0025F02:74.6m, measured starting from the fracture surface. The scan width was 0.9 mm.

The autoradiographs provided from rock surfaces sawn parallel to the fracture surface are shown in Figure. 3-49. The measured porosity histogram from the first autoradiograph taken at a depth of 2 mm from the fracture surface is presented in Figs. 3-50. At this depth highly porous phases were found; up to 8-10 %. The porosity pattern was heterogeneous, but no clearly visible cracks were found.

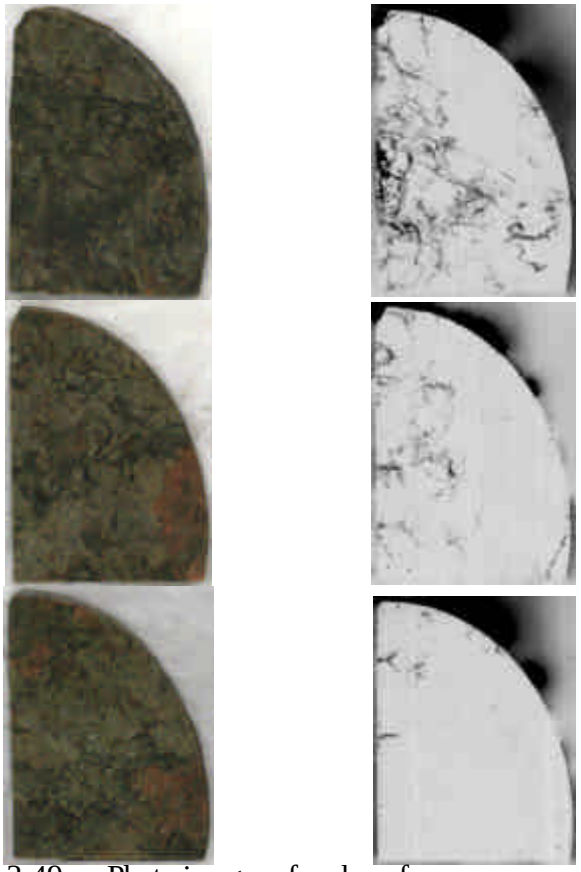

Figure 3-49. Photo images of rock surfaces sawn parallel to fracture surface (left) and corresponding autoradiographs (right, 13 d exposure). Depth from the fracture surface is shown in the far right column.

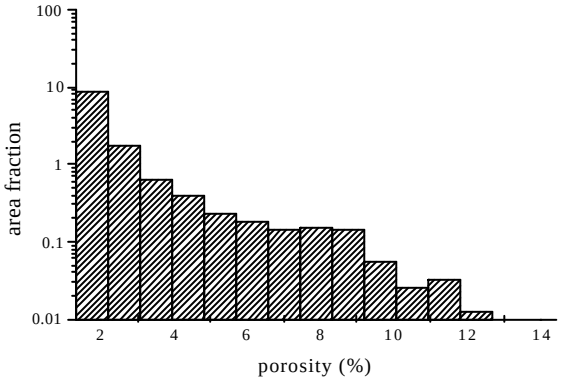

Figure 3-50. Porosity distribution presented as PMMA histograms provided from autoradiograph taken of first rock surface at a depth of 2 mm from fracture surface shown in Figure 3-49.

3.3.6 #20 KA2563:188.7m

Experimental conditions for the wall rock sample from intercept structure #20 in KA2563:188.7m are presented in a table in Appendix 3. The wall rock sample structure #20 in KA2563:188.7m was not impregnated thoroughout with MMA and one piece of the sample was impregnated twice (188.7 II). The sample was sawn according to the partition diagraphs shown in Figures 3-51 and 3-52.

Figure 3-51. Wall rock sample structure #20 in KA2563:188.7m sawn perpendicular to fracture surface for autoradiography to provide profile measurements.

Figure 3-52. Wall rock sample I structure #20 in KA2563:188.7m sawn parallel to fracture surface for autoradiography to provide porosity histograms at different depths.

As shown in autoradiograph of rock sample I structure #20 in KA2563:188.7m in Fig. 3-53, the rock matrix is very dense adjacent to the fracture surface. The nonporous zone is about 2 cm in width. A few cracks and fissures were found. A porous vein transsect the sample. The porosity distribution is shown in two histograms in Fig. 3-54. A feldspar area (region A) showed anomalous porosity; 0.35 and up to 8-10 % porosity was measured. Dark mineral areas had total porosity of 0.2 %, and local porosities of up to 4-5 % were measured.

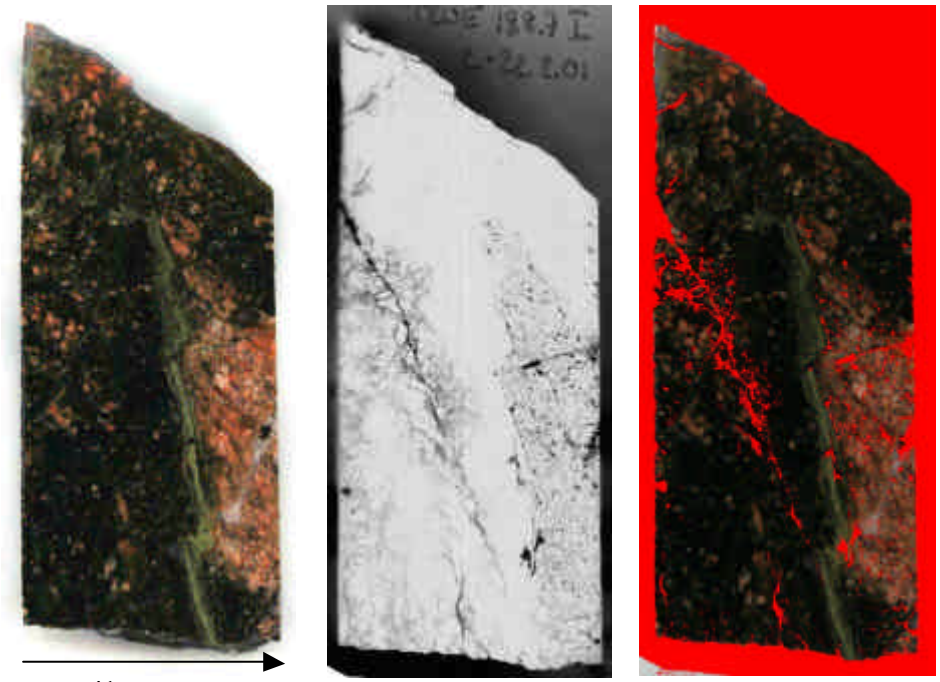

Figure 3-53. Photograph of wall rock sample I structure #20 in KA2563:188.7m (left), corresponding autoradiograph (center) (20 d exposure) and superimposed image (right) showing porous areas >0.5 % porosity (red).

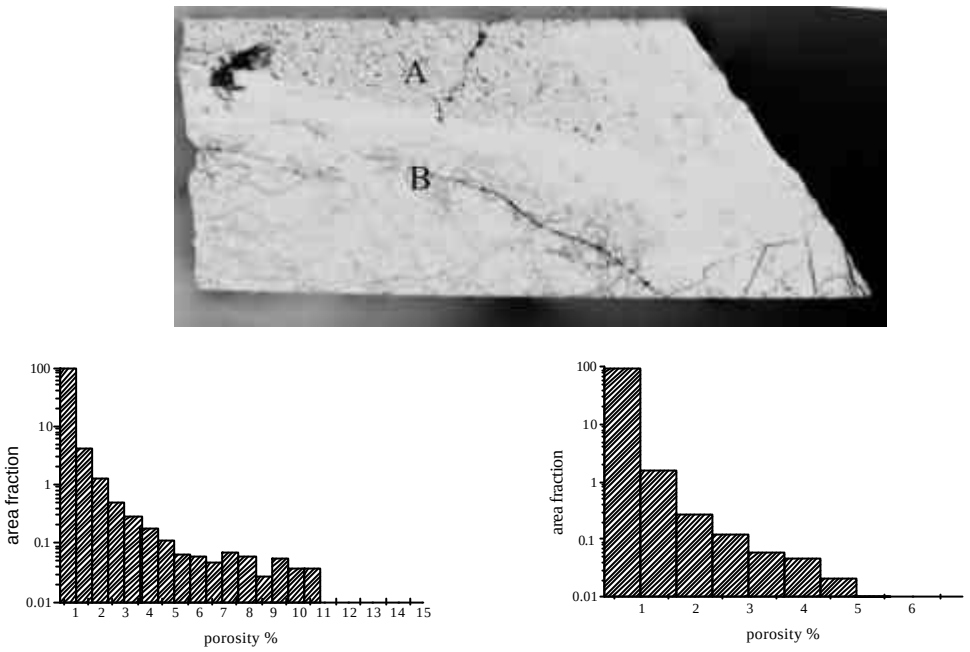

A (0.35 %) B (0.22 %)

Figure 3-54. Autoradiograph of sample I structure #20 in KA2563:188.7m showing areas of porosity measurements. Histograms showing porosity distribution in measured regions.

One autoradiograph provided from rock surfaces sawn parallel to the fracture surface is shown in Fig. 3-55. No cracks or fissures observed, the matrix is nonporous with the PMMA method.

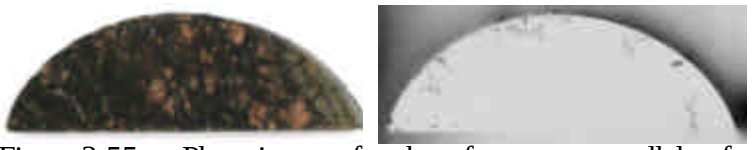

4.5 mm

Figure 3-55. Photo image of rock surfaces sawn parallel to fracture surface (left), corresponding autoradiograph (center, 14 d exposure).
Depth from the fracture surface is shown in the far right column.

4. Conclusions and discussion

Interconnected porosity, microfracturing and porosity profiles next to water conducting fractures of altered Äspö diorite samples from the interpreted deterministic structures at TRUE Block Scale Site were studied by using the ^{14}C- and the ^{3}H-PMMA methods. The heterogeneities in the porosity distribution could be visualized in the three categories of rock samples: fault breccia fragments (1-2 mm), fault breccia pieces (1-3 cm) and wall rock samples.

The PMMA method was tested here to study the porosity and microfracturing of the fault breccia fragments having particle sizes of 0.5 to 2 mm. Some of the rock fragments were easily impregnated with MMA and the method worked. It is recommended to use the particle sizes above 1 mm. The resolution of the autoradiographs was good enough to reveal the porosity distribution of the fragments, especially the autoradiographs provided with ^{3}H labelled PMMA. The digitizing of the autoradiographs has to be performed using higher resolution than 600 dpi to utilize all information from the autoradiographs. The CCD camera which is used through the microscope to digitize the autoradiographs would improve the results of the fragments. The fault breccia pieces were easily impregnated with ^{14}C-MMA. The ^{14}C-PMMA autoradiographs revealed the structures of this sample type effectively.

Six wall rock samples were impregnated with ^{14}C-MMA. There were problems in the impregnation. Very tight altered mineral phases proved to be nonporous with the PMMA method. MMA does not intrude into the pores, if the drying process has not been effective enough to remove all the porewater from the narrow pores of the minerals. The drying temperature varied from 70 to 90 °C in this study. To be sure that the porewater is removed and to avoid the problems, the drying temperature of rock samples should be increased to at least 105 °C [11]. This drying temperature is used in standard water gravimetric porosity measurements. Another reason for unsatisfactory results could be too short impregnation time. The impregnation time that ranged between 5 to 7 days could be increased to 2 or 3 weeks. The impregnation times and drying temperatures were chosen according to the earlier work experience of this size fresh granitic rocks, where the problems had not arisen.

REFERENCES

1. Byegård, J., Widestrand, H., Skålberg, M., Tullborg, E-L. and Siitari-Kauppi, M. (2001). First TRUE stage. Comlementary Investigations of Diffusivity, Porosity and Sorbitivity of Feature A Site-specific Geological Material, Swedish Nuclear Fuel and Waste Management Company, Äspö Hard Rock Laboratory, International Cooperation Report ICR-01-04

2. Andersson, P., Byegård, J., Doe, T., Hermanson, J., Meier, P., Tullborg, E-L. and Winberg, A. (in prep.). Final Report of the TRUE Block Scale Project – 1. Characterisation and Model Development, SKB Technical Report TR-XX-XX

3. Autio, J., Kirkkomäki, T., Siitari-Kauppi, M., Laajalahti, M., Aaltonen, T. and Maaranen, M. (1999). Use of the ^{14}C-PMMA and He-gas Methods to Characterise Excavation Disturbance in Crystalline Rock, Posiva 99-22

4. Siitari-Kauppi, M. (1995). Investigation of Porosity and Microfracturing in a Disturbed Zone with the ^{14}C-PMMA Method Based on Samples from Full-Scale Experimental Deposition Holes of the TVO Research Tunnel, Nuclear Waste Commission of Finnish Power Companies, Report YJT-95-13 & Arbets Rapport AR D-96-001

5. Hellmuth, K.H., Siitari-Kauppi, M. and Lindberg, A. (1993). Study of Porosity and Migration Pathways in Crystalline Rock by Impregnation with ^{14}C-polymethylmethacrylate, Journal of Contaminant Hydrology, 13: 403-418

6. Hellmuth, K.H., Lukkarinen, S. and Siitari-Kauppi, M. (1994). Rock Matrix Studies with Carbon-14-Polymethylmethacrylate (PMMA); Method Development and Applications. Isotopenpraxis Environ. Health Stud., 30: 47-60

7. Siitari-Kauppi, M., Flitsiyan, E.S., Klobes, P., Meyer, K., Hellmuth, K-H. (1998). Progress in physical rock matrix characterization: structure of the pore space, In: I.G. McKinley, C. McCombie (edits.), Scientific Basis for Nuclear Waste Management XXI, Mat. Res. Soc. Symp. Proc. 506: 671-678

8. Daniels, F. and Alberty, R. A. (1967). Physical Chemistry, Third Edition, John Wiley & Sons, Inc. New York, 767: 384

9. Leonard, E. C. (1978). Vinyl and Diene Monomers, Part 1, A Series of Monographs on the Chemistry, Physics, and Technology of High Polymeric Substances, XXIV: 157

10. Evans, R. D. (1955) The Atomic Nucleus, McGraw-Hill Book Company, NY, 621-629

11. Suggested Methods for Determining Water Content, Porosity, Density, Absorption and Related Properties and Swelling and Slake-durability Index Properties, International Society for Rock Mechanics, In: Rock Characterization, Testing and Monitoring ISRM Suggested Methods, Pergamon Press 1979, 81-84

APPENDICES

APPENDIX 1 (1)

^{14}C-PMMA Fault breccia fragments' experimental procedure

code	diameter (mm)	code in experiment	weight (g)	priority	drying (time/temp)	tracer activity	impregnation	radiation dose	polishing	autoradiography
#22 KI0025F02:**66.7**	0.5-1.0	test 1	0.0758	1	1 d / 120 °C	0.7 µCi/ml	1 d	76 kGy	1.	1.exposure 2 d 2.exposure 14 d
	0.5-1.0	test 2	0.1254	1	3 d / 120 °C	0.7 µCi/ml	1 d	26 kGy	1.	1.exposure 1 d 2.exposure 14 d
									2.	1.exposure 5 d
	1-2	test 3	0.6533	1	2 d / 120 °C	1.2 µCi/ml	1 d	79 kGy	1.	1.exposure 7 d 2.exposure 12 d
									2.	1.exposure 2 d
									3.	1.exposure 5 d
									4.	1.exposure 2 d
	1-2	test 4	0.2077	1	2 d / 120 °C	25 µCi/ml	1 d	71 kGy	1.	1.exposure 4 d
									2.	1.exposure 2 d
									3.	1.exposure 5 d
									4.	1.exposure 2 d

APPENDIX 1 (2)

^{3}H-PMMA Fault breccia fragments' experimental procedure

code	diameter (mm)	code in experiment	weight (g)	priority	drying (time/temp)	tracer activity	impregnation	radiation dose	polishing	autoradiography
#22 KI0025F02:**66.7**	1-2	test 5	0.2319	1	7 d / 120 °C	3 mCi/ml	2 d	105 kGy	1.	1.exposure 2 d
									2.	1.exposure 2 d 2.exposure 2 d
									3.	1.exposure 5 d 2.exposure 2 d
#20 KI0023B:**69.9**	0.5-1.0	test 6	0.0731	3	1 d / 120 °C	3 mCi/ml	1 d	124 kGy	1.	1.exposure 2 d
									2.	1.exposure 2 d
									3.	1.exposure 5 d 2.exposure 2 d
	1-2	test 7	0.1607	3	1 d / 120 °C	3 mCi/ml	1 d	75 kGy	1.	1.exposure 2 d
									2.	1.exposure 5 d 2.exposure 2 d

APPENDIX 2

^{14}C-PMMA Fault breccia pieces' experimental procedure

code	weight	priority	drying (time/temp)	tracer activity	impregnation	radiation dose
A						
#22 KI0025F02:**66.7**	11.95 g	1	3 d / 75 °C	25 µCi/ml	4 d	50 kGy
#20 KI0023B:**69.9**	10.58 g	3	3 d / 75 °C	25 µCi/ml	4 d	50 kGy
B						
#22 KI0025F02:**66.7**	1.46 g	1	3 d / 120 °C	0.7 µCi/ml	1 d	100 kGy
#20 KI0023B:**69.9**	5.01 g	3	3 d / 120 °C	0.7 µCi/ml	1 d	100 kGy

code		autoradiography	code		autoradiography
#22 KI0025F02:**66.7**	**A-B**	1.exposure 5 d 2.exposure 9 d	#20 KI0023B:**69.9**	**A-B**	1.exposure 5 d 2.exposure 9 d
	A-C	1.exposure 4 d 2.exposure 9 d		**A-C**	1.exposure 4 d 2.exposure 9 d
	A-D	1.exposure 4 d 2.exposure 5 d 3.exposure 6 d		**A-D**	1.exposure 4 d 2.exposure 9 d
	B	1.exposure 7 d 2.exposure 12 d		**A-E**	1.exposure 5 d 2.exposure 9 d
				A-F	1.exposure 7 d
				B	1.exposure 7 d 2.exposure 12 d

APPENDIX 3 (1)

^{14}C-PMMA wall rock samples' experimental procedure

code	length (mm)	diameter (mm)	priority	drying (time/temp)	tracer activity (mCi/ml)	impregnation (time)	radiation (dose)	autoradiography
#22 KI0025F02:**66.7m**	50	51	1	6 d / 90 °C	25	7 d	100 kGy	1.exposure 3 d 2.exposure 10 d
2.impregnation (III)				7 d / 70 °C	25	9 d	60 kGy	1.exposure 10 d
#23 KI0025F03:**56.8m**	20	51	2	6 d / 90 °C	25	7 d	100 kGy	1.exposure 3 d 2.exposure 10 d
2.impregnation (II)				7 d / 70 °C	25	9 d	60 kGy	1.exposure 9 d 2.exposure 18 d
#20 KI0023B:**69.9m**	100	51	3	6 d / 90 °C	25	7 d	100 kGy	1.exposure 3 d 2.exposure 10 d
2.impregnation (I)				7 d / 70 °C	25	9 d	60 kGy	1.exposure 10 d
#21 KI0023F:**71.1m**	80	51	4	4 d / 70 °C	25	10 d	65 kGy	1.exposure 7 d 2.exposure 14 d
#20 KI0025F02:**74.6m**	55	51	5	5 d / 90 °C	25	10 d	110 kGy	1.exposure 6 d 2.exposure 14 d
#20 KA2563:**188.7m**	85	41	6	5 d / 90 °C	25	10 d	110 kGy	1.exposure 7 d 2.exposure 14 d
2.impregnation (II)				6 d / 90 °C	25	10 d	90 kGy	1.exposure 14 d

APPENDIX 3 (2)

The succession of impregnation and exposure employed to the ”66.7m wall rock” sample

#22 KI0025F02:**66.7**		**autoradiography**
1.impregnation	**I-A**	1.exposure 3 d 2.exposure 10 d
	I-B	1.exposure 15 d
	I-C	1.exposure 15 d
fractured surface A	**I-1a**	1.exposure 14 d
	I-2a	1.exposure 14 d 2.exposure 8 d
	I-2b	1.exposure 8 d 2.exposure 10d
	I-3a	1.exposure 14 d 2.exposure 8 d
	I-3b	1.exposure 8 d 2.exposure 10d
	II-A	1.exposure 3 d 2.exposure 10 d
	II-C	1.exposure 14 d
	II-D	1.exposure 15 d
	II-E	1.exposure 15 d
fractured surface B	**II-1a**	1.exposure 10 d
	II-2a	1.exposure 10 d
	II-3a	1.exposure 10 d
	II-4b	1.exposure 10 d
	III	1.exposure 3 d 2.exposure 10 d
2.impregnation	**III-A**	1.exposure 9 d 2.exposure 18 d
	III-B	1.exposure 9 d 2.exposure 18 d

APPENDIX 3 (3)

The succession of impregnation and exposure employed to the ”56.8m and 69.9m wall rock” samples

#23 KI0025F03:**56.8**		**autoradiography**	#20 KI0023B:**69.9**		**autoradiography**
1.impregnation	**I-A**	1.exposure 3d 2.exposure 10d	1.impregnation	**I**	1.exposure 3 d 2.exposure 10 d
	I-B	1.exposure 15d		**I-1a**	1.exposure 10 d
	I-C	1.exposure 15d		**I-2a**	1.exposure 10 d
	II	1.exposure 10d		**I-3a**	1.exposure 10 d
				I-4b	1.exposure 10 d
				II	1.exposure 3 d 2.exposure 10 d 3.exposure 14 d
2.impregnation	**II-A**	1.exposure 9d 2.exposure 18d	2.impregnation	**I-A**	1.exposure 9 d 2.exposure 20 d
	II-B	1.exposure 9d 2.exposure .18d		**I-B**	1.exposure 9 d 2.exposure 20 d
	II-1a	1.exposure 13d			
	II-2a	1.exposure 13d			
	II-3a	1.exposure 13d			
	II-4b	1.exposure 13d			

APPENDIX 3 (4)

The succession of impregnation and exposure employed to the ”71.1m, 74.6m and 188.7m wall rock” samples

#21 KI0023F:**71.1**	**autoradiography**	#20 KI0025F02:**74.6**	**autoradiography**	#20 KA2563:**188.7**	**autoradiography**
I	1.exposure 7 d 2.exposure 14 d	**I**	1.exposure 6 d 2.exposure 14 d	**I**	1.exposure 7 d 2.exposure 14 d 3.exposure 20 d
I-1a	1.exposure 14 d	**I-1a**	1.exposure 10 d	**I-1a**	1.exposure 14 d
I-2a	1.exposure 14 d	**I-2a**	1.exposure 10 d	**I-2a**	1.exposure 14 d
I-3a	1.exposure 14 d	**I-3a**	1.exposure 10 d	**I-3a**	1.exposure 14 d
		I-4b	1.exposure 10 d		
II	1.exposure 7 d 2.exposure 14 d 3.exposure 20 d	**II**	1.exposure 6 d 2.exposure 14 d	**II**	1.exposure 7 d 2.exposure 14 d 3.exposure (2.imp) 14 d

APPENDIX 4 (1)

Fault breccia fragments, ^{14}C-PMMA impregnated (5 days exposure)

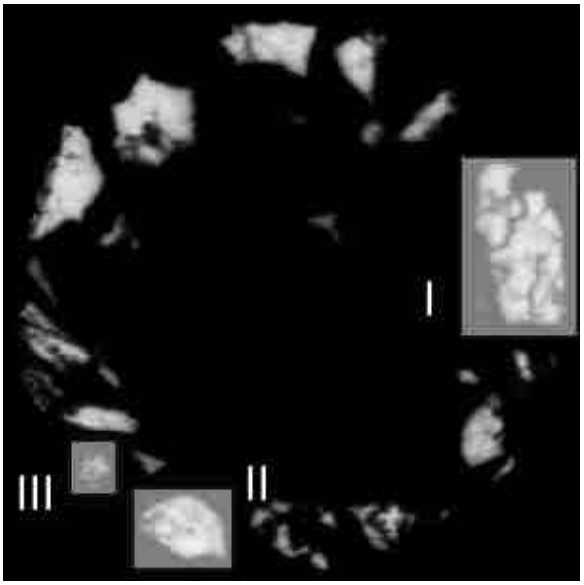

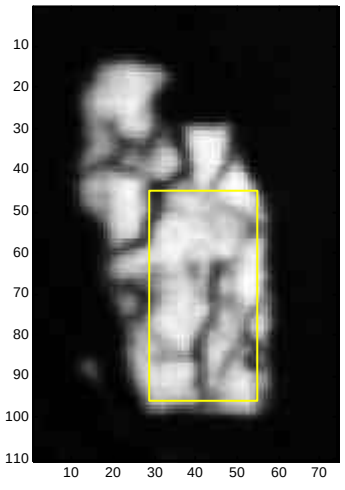

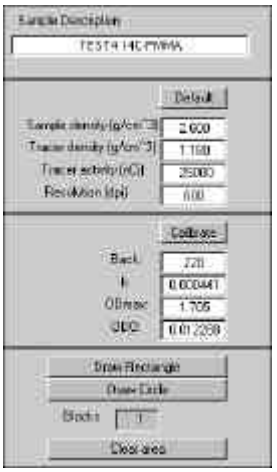

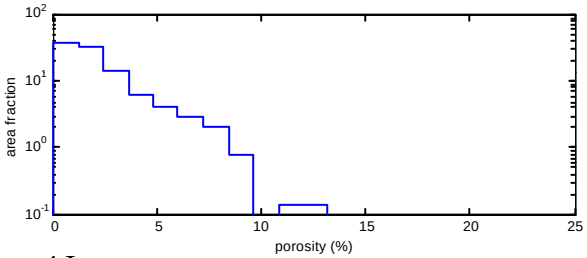

test4 I

APPENDIX 4 (2)

Fault breccia fragments, ^{14}C-PMMA impregnated (5 days exposure)

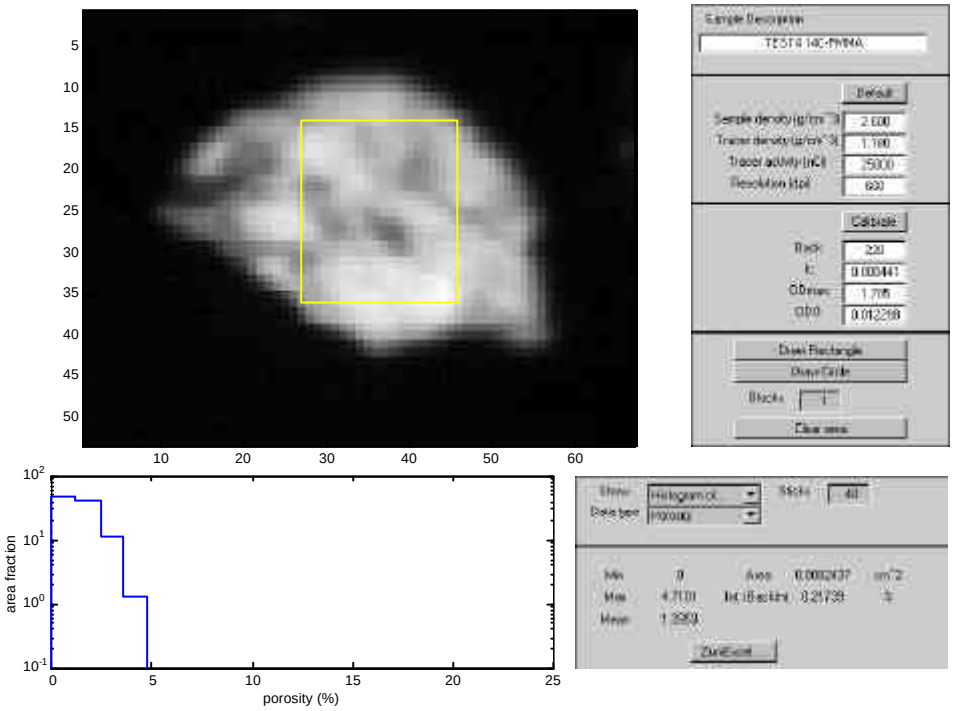

test4 II

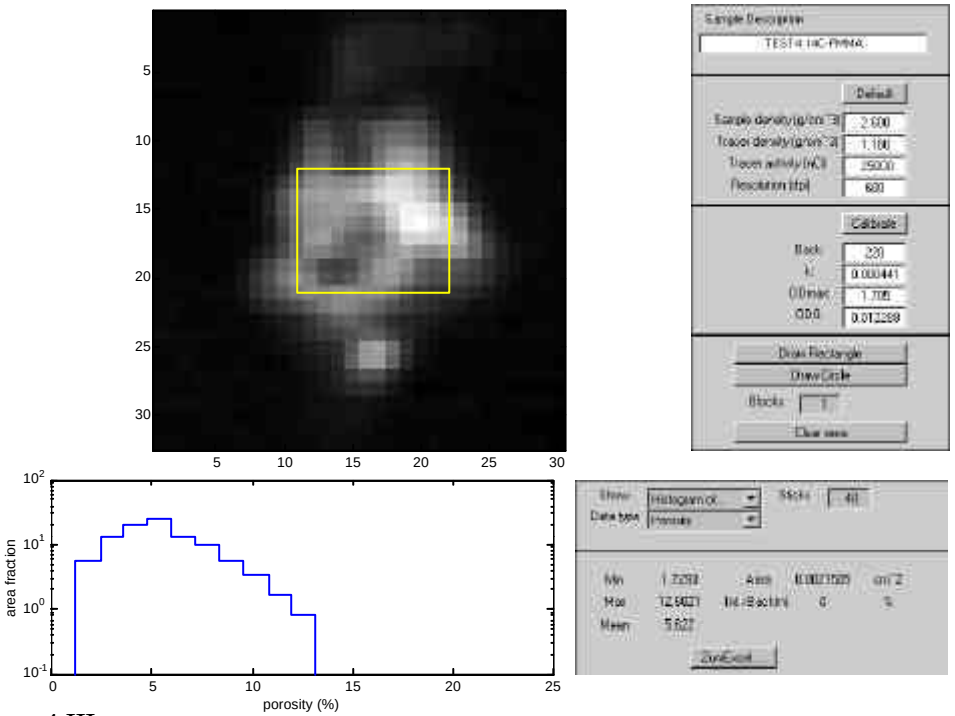

test4 III

APPENDIX 5 (1)

Fault breccia fragments, ^{3}H-PMMA impregnated (5 days exposure)

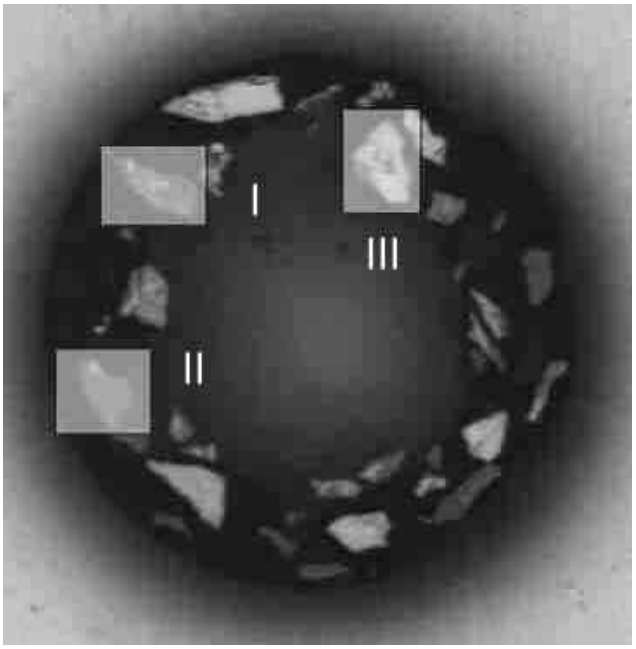

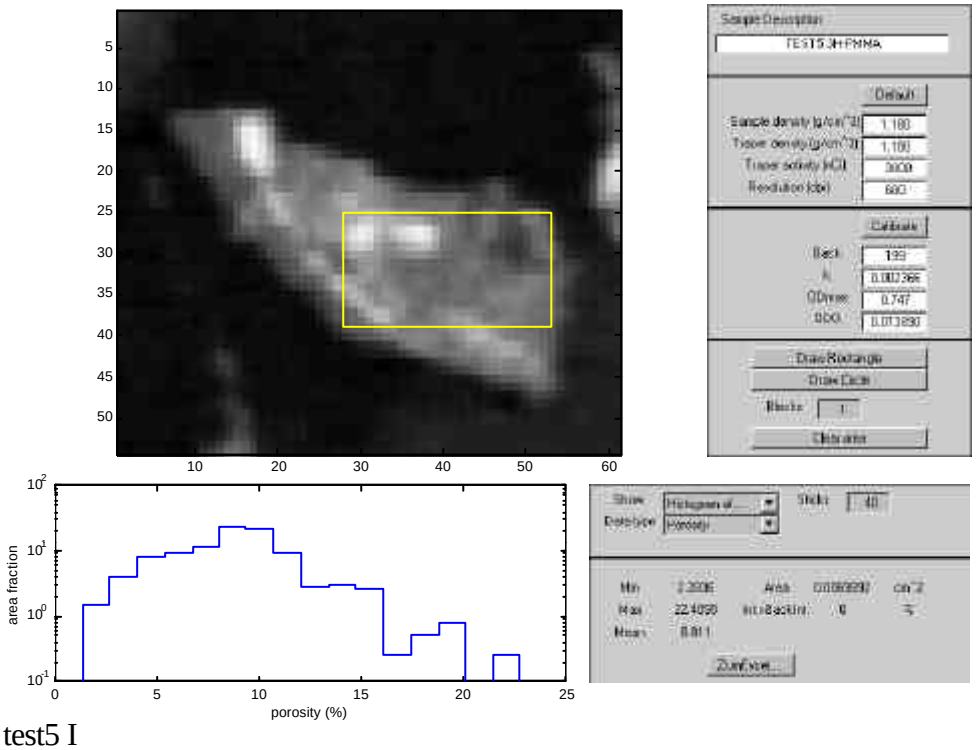

test5 I

APPENDIX 5 (2)

Fault breccia fragments, ^{3}H-PMMA impregnated (5 days exposure)

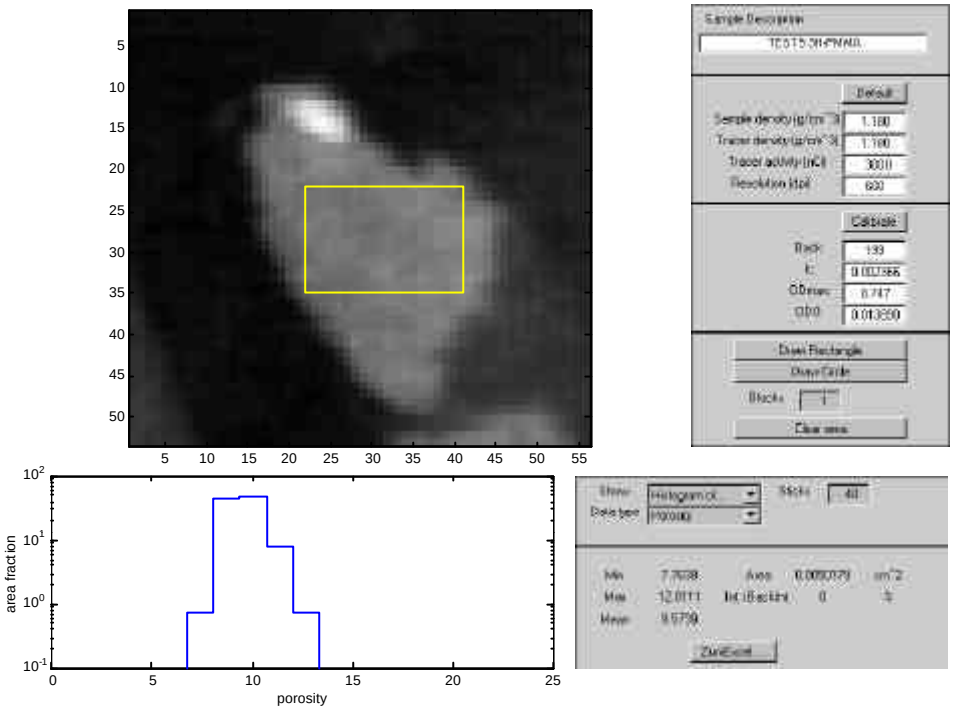

test5 II

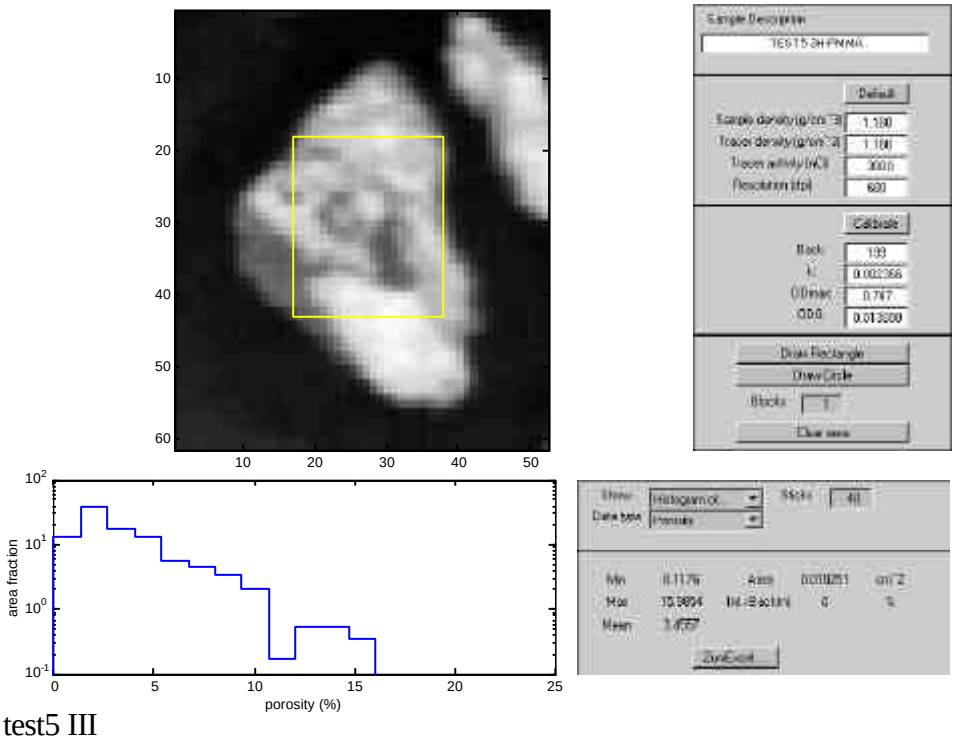

test5 III

APPENDIX 6 (1)

Fault breccia fragments, ^{3}H-PMMA impregnated (5 days exposure)

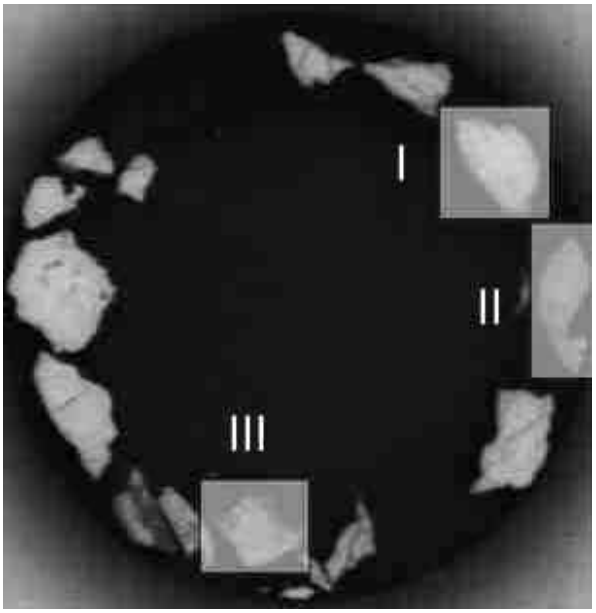

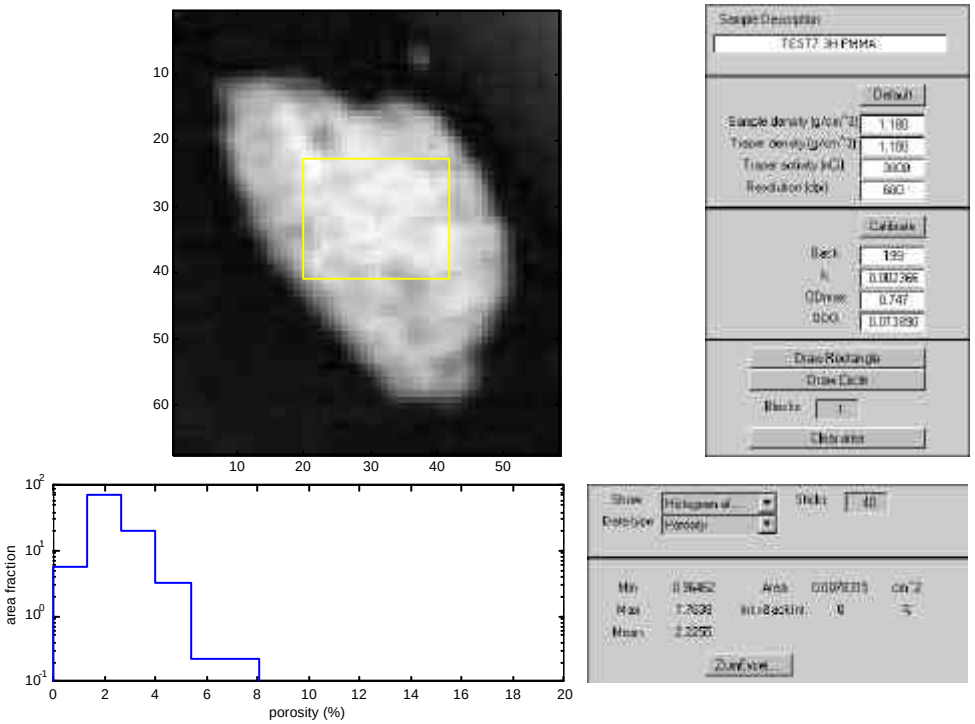

test7 I

APPENDIX 6 (2)

Fault breccia fragments, ^{3}H-PMMA impregnated (5 days exposure)

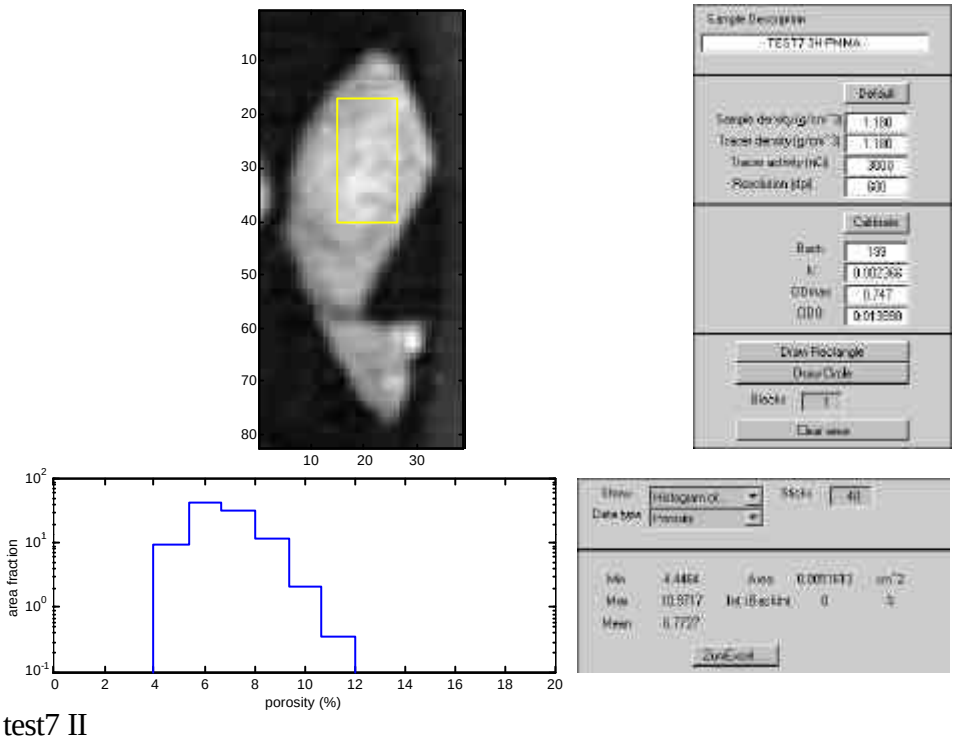

test7 II

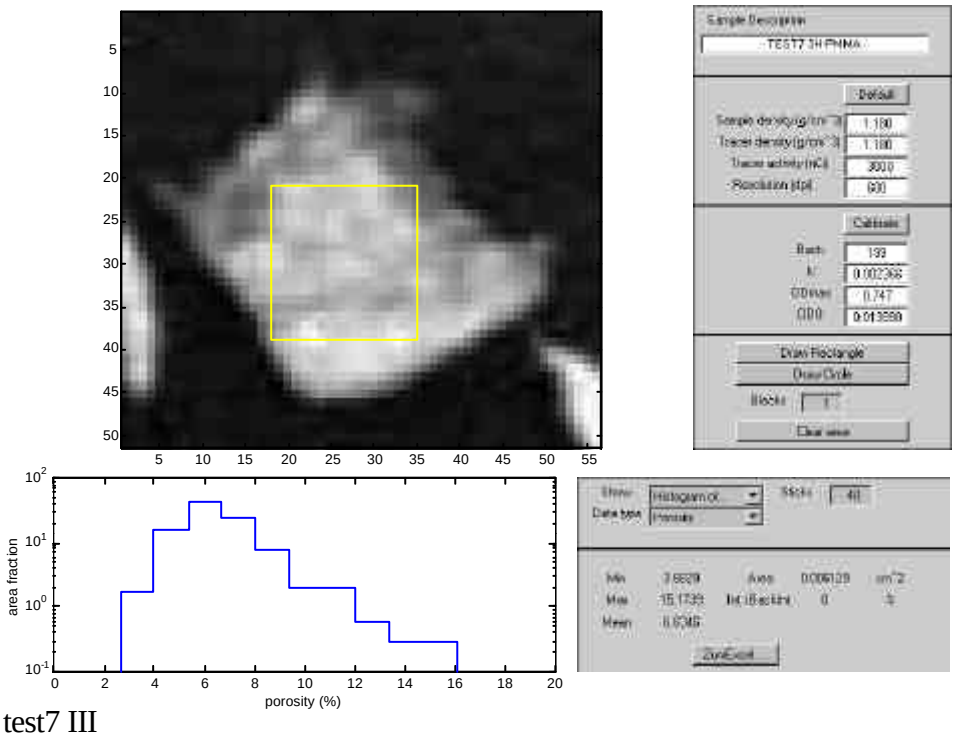

test7 III